Eur. Phys. J. C 52, 55–74 (2007)
DOI 10.1140/epjc/s10052-007-0389-1

THE EUROPEAN PHYSICAL JOURNAL C

Regular Article – Experimental Physics

A study in depth of $f_0(1370)$

D.V. Bugg[a]

Queen Mary, University of London, London E1 4NS, UK

Received: 5 June 2007 / Revised version: 18 July 2007 /
Published online: 13 August 2007 –

Abstract. Claims have been made that $f_0(1370)$ does not exist. The five primary sets of data requiring its existence are refitted with suitable Breit–Wigner amplitudes. Major dispersive effects due to the opening of the 4π threshold are included for the first time; the $\sigma \to 4\pi$ amplitude plays a strong role. Crystal Barrel data on $\bar{p}p \to 3\pi^0$ at rest require $f_0(1370)$ signals of at least 32 and 33 standard deviations (σ) in $^1S_0$ and $^3P_1$ annihilation respectively. Furthermore, they agree within 5 MeV for mass and width. Data on $\bar{p}p \to \eta\eta\pi^0$ agree and require at least a 19σ contribution. This alone is sufficient to demonstrate the existence of $f_0(1370)$. BES II data for $J/\Psi \to \phi\pi^+\pi^-$ contain a visible $f_0(1370)$ signal $> 8\sigma$. In all cases, a resonant phase variation is required. Cern–Munich data for $\pi\pi$ elastic scattering are fitted well with the inclusion of some mixing between σ, $f_0(1370)$ and $f_0(1500)$. Values of $\Gamma_{2\pi}$ for $f_2(1565)$, $\rho_3(1690)$, $\rho_3(1990)$ and $f_4(2040)$ are determined.

PACS. 13.25.Gv; 14.40.Gx; 13.40.Hq

1 Introduction

The $f_0(1370)$ plays a vital role in the spectroscopy of light $J^P = 0^+$ mesons. The role of experiment is to identify the resonances required by data and determine their parameters: mass, width and branching ratios. Many schemes exist for grouping the observed states into nonets. The 0^+ glueball is predicted at ~ 1640 MeV [1], but with a sizable error from uncertainty in how to normalise the mass scale. The glueball would make an additional SU(3) singlet state, mixing with neighbouring nonet states. It is therefore necessary to scrutinise the evidence for each state.

Klempt [2] and Klempt and Zaitsev [3] question whether there is an identifiable 0^+ glueball and hence argue against the existence of $f_0(1370)$. Ochs has argued against it at conferences for two reasons. He suggests that it can be confused with a broad 'background' which might obscure the analysis of the 1000–1500 MeV mass range [4, 5]; secondly he argues that it has not been identified definitively in Cern–Munich data [4, 5]. The weakness of these arguments is that no attempt has been made to refit the data where $f_0(1370)$ has been identified. The main objective of the present work is to do just that.

The earliest evidence for the $f_0(1370)$ came from experiments on $\pi\pi \to KK$ at the Argonne and Brookhaven laboratories in the late 1970's. A peak was observed in the S-wave at 1300 MeV in three sets of data: Cohen et al. [6], Pawlicki et al. [7] and Etkin et al. [8]. In those days it was called the $\epsilon(1300)$. Further evidence appeared in the years 1992–96 from several experiments in quick succession. Amsler et al. reported a peak in the $\eta\eta$ S-wave at ~ 1400 MeV in Crystal Barrel data on $\bar{p}p$ annihilation at rest into $\eta\eta\pi^0$ [9] (as well as a further peak at 1560 MeV, later identified as $f_0(1500)$). Gaspero reported a 0^+ state in 4π at 1386 ± 30 MeV in $\bar{p}d$ bubble chamber data at rest in the reaction $\bar{p}n \to 2\pi^+3\pi^-$ [10]; the Obelix collaboration quickly confirmed this observation in $\bar{n}p \to 3\pi^+2\pi^-$ [11], quoting a mass of 1345 ± 12 MeV. Crystal Barrel reported a similar 0^+ state in 4π at 1374 ± 38 MeV in $\bar{p}p$ annihilation at rest to $(\pi^+\pi^-\pi^0\pi^0)\pi^0$ [12].

The earliest fits in which $f_0(1370)$ and $f_0(1500)$ appeared together were made using early low statistics Crystal Barrel data on $\bar{p}p \to 3\pi^0$ at rest [13–15]. Publications using the full statistics data (used here) appeared in 1995 [16] and 1996 [17]. The latter work involved a simultaneous fit [18] to Cern–Munich data on $\pi\pi \to \pi\pi$ [19] and data on $\pi\pi \to KK$. The observation of nearby $f_0(1370)$ and $f_0(1500)$ states, both dominantly non-strange, excited interest in the 0^+ glueball. Further extensive studies of $f_0(1370)$ and $f_0(1500)$ by Crystal Barrel, Obelix and Omega collaborations may be traced via the Particle Data tables [20].

The present work fits simultaneously the 5 most definitive sets of data available to me. The first two are Crystal Barrel data on $\bar{p}p \to 3\pi^0$ at rest in liquid hydrogen [17] and gaseous hydrogen. These two sets of data allow a clean separation of annihilation from $^1S_0$ and $^3P_1$ $\bar{p}p$ states: P-state annihilation is $\sim 13\%$ in liquid and 48% in gas. The combined fit also includes two sets of data for $\bar{p}p \to \eta\eta\pi^0$ in liquid and gas. There are visible $f_0(1370)$ and $f_0(1500)$ peaks in both of these sets of data. The fifth definitive set of data comes from BES II for $J/\Psi \to \phi\pi^+\pi^-$. There is

[a] email: D.V.Bugg@rl.ac.uk

a visible $\pi\pi$ peak at 1350 MeV, attributed to interference between $f_0(1370)$, $f_0(1500)$ and $f_2(1270)$ [21]. Those data are refitted with and without inclusion of $f_0(1370)$.

Finally, an earlier analysis fitted data on $\pi\pi \to KK$ and $\eta\eta$ [22]; this analysis also fitted Kloe data on $\phi \to \pi^0\pi^0\gamma$ and $\eta\pi^0\gamma$. The $\pi\pi \to KK$ data suggest the presence of $f_0(1370)$ but cannot be considered definitive compared with the other sets of data. This analysis remains consistent with parameters of $f_0(1370)$ found here.

The Particle Data Group quotes very large errors for mass and width of $f_0(1370)$: $(1200–1500) - \mathrm{i}(150–250)$ MeV. From the present analysis, the error on the mass is very small: ± 15 MeV from systematics. The resonance will still be referred to as $f_0(1370)$, despite the fact that its peak position in the $\pi\pi$ channel comes out nearly 100 MeV lower. The Particle Data Group appears to be influenced by large variations in masses and widths fitted to 4π data. These variations are due to the fact that there has been no serious attempt to include $\sigma \to 4\pi$ in these analyses. A major objective here is to treat fully the dispersive effects due to the opening of the 4π threshold, to which σ, $f_0(1370)$ and $f_0(1500)$ all couple strongly.

The full form of the Breit–Wigner resonance formula,

$$f = \frac{1}{M^2 - s - m(s) - \mathrm{i}M\Gamma_{\mathrm{total}}(s)} \tag{1}$$

contains a real dispersive term $m(s)$ [23], which for the 4π channel reads

$$m(s) = \frac{s - M^2}{\pi} \int \frac{\mathrm{d}s' M\Gamma_{4\pi}(s')}{(s'-s)(s'-M^2)}\,. \tag{2}$$

We shall find that $m(s)$ is large, indeed larger than $(M^2 - s)$ in the Breit–Wigner denominator. It turns out that this places severe limitations on the ratio $\Gamma_{2\pi}/\Gamma_{4\pi}$ which can be fitted to data. This point was not appreciated in earlier work. Nevertheless, a good solution emerges naturally.

Here there is an interesting conclusion. The fit includes explicitly the s-dependence of the 4π channel, as far as present data allow. However, the amplitude still produces an Argand diagram very close to a circle and hence similar to a simple pole. This justifies to some degree the common usage of a simple Breit–Wigner formula in fitting data.

A third point concerns the coupling to 4π by the broad component in the $\pi\pi$ S-wave related to the σ pole; this component will be called σ as a short-hand. It plays an essential role in fitting all data where a $\pi\pi$ pair is produced. Let us review the situation briefly.

The $\pi\pi$ S-wave phase shift reaches 90° at ~ 900 MeV. There is an Adler zero in the elastic amplitude at $s \simeq m_\pi^2/2$, just below the $\pi\pi$ threshold. The resulting amplitude rises approximately linearly with s. In production data from E791 [24] and BES II [25], a strong peak is observed at ~ 500 MeV. Both these production data and elastic scattering may be fitted with the same Breit–Wigner denominator, but with an s-dependent width and with different numerators for production and elastic cases; for elastic scattering, the numerator contains the Adler zero, whereas for the BES II production data fitted here it is consistent with a constant. The same variation of the phase shift with s is observed in elastic scattering and production data from 450 to 950 MeV within errors of $\sim 3.5^\circ$ [26]. The large displacement of the pole from 900 MeV arises from the s-dependence of the width; the Cauchy–Riemann relations control the s-dependence of the real and imaginary parts of the amplitude as one extrapolates from the physical s-axis.

The fit of [22] to $\pi\pi \to KK$ and $\eta\eta$ data and the Kloe branching ratio for $\phi \to \pi^0\pi^0\gamma$ determines ratios of coupling constants for the σ coupling to KK and $\eta\eta$: $g^2(KK)/g^2_{\pi\pi} = 0.6 \pm 0.1$ and $g^2_{\eta\eta}/g^2_{\pi\pi} = 0.2 \pm 0.05$. The remaining unknown is the coupling of σ to 4π. This will play an essential role in the work reported here.

A vital question is whether this coupling to 4π eliminates the requirement for the $f_0(1370)$. Tornqvist has suggested [27, 28] that a second pole could appear in the σ amplitude due to the opening of the 4π threshold. Could this explain $f_0(1370)$ as a non-$q\bar{q}$ state? A related point is that Maiani et al. have suggested that $f_0(1370)$ may be a molecular state [29].

The layout of the paper is as follows. Section 2 discusses the formalism and gives equations. Amplitudes are expressed in terms of T-matrices for reasons discussed there. This raises some issues concerning how to fit elastic scattering. Readers interested only in results may skip this section, but the issues going into the formulae are outlined in words for the general reader. It is important to add that extensive fits to Crystal Barrel and other data have been made by Anisovich and Sarantsev, using K-matrix techniques [30]. These analyses produce results closely similar to the present work, and there is no conflict between the two analyses: they should be regarded as complementary views. The K-matrix analyses use several sets of data not available to me, for example Crystal Barrel data on $\bar{p}p \to KK\pi$. Their conclusion is that $f_0(1370)$ is needed, with mass and width in close agreement to what is found here. However, they do not address the question of how much the fit changes if $f_0(1370)$ is omitted.

Section 3 is the heart of the paper, concerning fits to data with and without $f_0(1370)$. A suggestion made by Ochs is that the amplitude for the $\pi\pi$ S-wave should be fitted freely in magnitude and phase in bins of $\pi\pi$ mass, without assuming a Breit–Wigner form. Over the limited mass range 1100–1460 MeV, this is done and confirms the assumption of a resonance form for the amplitude.

Section 4 describes the simultaneous fit made to Cern–Munich data on $\pi\pi$ elastic scattering. They can be fitted slightly better with $f_0(1370)$ than without, but cannot be considered definitive on this question. Section 5 describes the fit to $\eta\eta\pi^0$ data; there is a visible peak in these data, sufficient alone to justify the existence of $f_0(1370)$.

Section 6 describes the fit to BES data on $J/\Psi \to \phi\pi^+\pi^-$. An important detail is that these data, together with data on $J/\Psi \to \omega\pi\pi$ [25] and ωKK [31] require the existence of an $f_0(1790)$ distinct from $f_0(1710)$. The $\phi\pi\pi$ data contain a clear $\pi\pi$ peak at 1790 MeV. Data on $\phi\pi\pi$ and ϕKK final states require a ratio $\mathrm{BR}[f_0(1790) \to \pi\pi]/\mathrm{BR}[f_0(1790) \to KK] > 3$ [21]. Data on $J/\Psi \to \omega KK$ contain a strong KK peak due to $f_0(1710)$; this peak is completely absent from $\omega\pi\pi$ data which require

$\mathrm{BR}[f_0(1710)\to\pi\pi]/\mathrm{BR}[f_0(1710)\to KK]<0.11$ with 95% confidence. A single resonance must have the same branching ratios in all sets of data, whereas these data differ in branching ratio by at least a factor 22. So two separate resonances are required. Unfortunately, the PDG ignores these decisive results and continues to lump $f_0(1790)$ with $f_0(1710)$. In the present fits to $\bar{p}p\to 3\pi^0$ data, $f_0(1790)$ is included together with $f_0(1370)$ and $f_0(1500)$, though its eventual contribution to the data is small.

Section 7 makes brief remarks on data for $\pi\pi\to KK$, and Sect. 8 remarks on the need for further analyses where the opening of thresholds leads to large dispersive effects. Section 9 makes concluding remarks.

2 Discussion of formulae

There are two obvious ways of expressing amplitudes, using K-matrices or T-matrices. Each has some advantages, but also limitations. It seems likely that neither is perfect, so approximations are needed in either case.

Resonances appear directly as poles of the T-matrix. The $\pi\pi$ S-wave is of primary concern. For this amplitude, K-matrix poles are displaced strongly from T-matrix poles. For elastic scattering, $K\propto\tan\delta$ (where δ is the phase shift), and K-matrix poles are at ~ 700 and 1200 MeV, whereas the $f_0(980)$ pole is at $998-\mathrm{i}17$ MeV.

In fitting production data, e.g. $\bar{p}p\to 3\pi^0$, it is obviously advantageous to use T-matrices, because resonances are T-matrix poles. The primary objective of the present work is to test whether the $f_0(1370)$ is needed or not. It is necessary to move its mass, width and couplings to all decay channels in steps, so as to examine the effect on χ^2. This cannot be done readily using K-matrices, since the $f_0(1370)$ is built out of a combination of K-matrix poles. It is also necessary to remove $f_0(1370)$ from the fit and again test χ^2. This cannot be done in a controlled way using K-matrix poles: if one K-matrix pole is removed, all resonances are affected. For this reason, amplitudes will be written directly in terms of T-matrices.

There is a second related point. It is well known that minimisation routines converge best when expressed in terms of eigenvectors, i.e. T-matrix poles. Weak or questionable resonances appear as weak eigenvectors and can be recognised immediately from the error matrix of the fit.

Yet another consideration is that earlier work fitting the σ pole and Cern–Munich data was done using T-matrices [32]. The formulae used there are readily expanded to incorporate the 4π channel. Also Ref. [22] fitted data on $\pi\pi\to KK$ and $\eta\eta$ and also Kloe data with T-matrices; it is valuable to maintain consistency with that analysis, for comparison of results.

2.1 Elastic scattering

There are however questions about how to deal with elastic scattering. Below the KK threshold, the amplitude is confined to the unitary circle. Both $f_0(980)$ and σ contribute, as do the low mass tails of further resonances. Experiment shows directly how to treat the overlap of these resonances. In Cern–Munich data, the $\pi\pi$ phase shift rises dramatically near 1 GeV from ~ 90 to 270° due to the narrow $f_0(980)$. The appropriate treatment below the KK threshold is to add phases, hence multiply S-matrices: $S=\exp(2\mathrm{i}\delta)$.

Above the inelastic threshold, multiplying S-matrices gives a fit of rather indifferent quality. It is clear that other factors must be relevant. If one solves a relativistic Schrödinger equation using a trial potential which reproduces σ, $f_0(980)$ and $f_0(1370)$, the solution is automatically unitary and analytic. One finds that amplitudes differ from both (i) the product of individual T-matrices for each resonance, (ii) the sum of K-matrices. Neither gives an accurate parametrisation. The main problem appears to be that resonances mix via processes of the form $<\sigma|\pi\pi|f_0>$ or other intermediate channels KK, $\eta\eta$, etc. Mixing is strong for elastic scattering, since the amplitudes are at the unitary limit when one takes account of all channels. The mixing gives rise to well known level-repulsion. This repulsion is still highly significant one full-width away from the resonance mass.

Formulae for mixing have been given by Anisovich, Anisovich and Sarantsev [33] and will be reproduced here in a slightly modified notation. For the 2-resonance case, the denominator $D(s)$ of one resonance may be written

$$D_{11}(s)=M_1^2-s-m_1(s)-\mathrm{i}M_1\Gamma_1^{\mathrm{tot}}(s) -\frac{B_{12}(s)B_{21}(s)}{M_2^2-s-m_2(s)-\mathrm{i}M_2\Gamma_2^{\mathrm{tot}}(s)}\,. \tag{3}$$

Mixing arises via B_{12} which in general is complex and may be s-dependent. The propagator matrix describing two resonances is then

$$\begin{aligned}\hat{D}&=\begin{vmatrix}D_{11}&D_{12}\\D_{21}&D_{22}\end{vmatrix}\\&=\frac{1}{(M_1^2-s-m_1(s))\,(M_2^2-s-m_2(s))}\\&\quad\times\begin{vmatrix}M_2^2-s-m_2(s)&B_{12}\\B_{21}&M_1^2-s-m_1(s)\end{vmatrix}\,.\end{aligned} \tag{4}$$

Because σ overlaps strongly with $f_0(980)$, $f_0(1370)$ and $f_0(1500)$, this mixing has been included explicitly in fitting elastic data. It turns out that inclusion of mixing between these pairs of states leads to an excellent fit using constant values of B_{12}.

It is also instructive to expand the denominator of the last term of (4) off resonance using the binomial theorem. The result is

$$D_{11}(s)=\left[M_1^2-s-m_1(s)-\mathrm{i}M_1\Gamma_1^{\mathrm{tot}}\right] -\frac{B_{12}B_{21}}{M_2^2-s}\left(1+\frac{m_2(s)+\mathrm{i}M_2\Gamma_2^{\mathrm{tot}}}{M_2^2-s}\right)\,. \tag{5}$$

From the last term, one gets contributions of the same sign to $\mathrm{Re}\,D_{11}(s)$ and $\mathrm{Im}\,D_{11}(s)$, while from the first term $[M_1^2-s-\mathrm{i}m_1-\mathrm{i}M_1\Gamma_1^{\mathrm{tot}}]$ contributions have opposite signs. The result is to rotate the phase of the amplitude, which derives purely from $D(s)$. This rotation is

large when resonances overlap strongly. Unless the mixing is included explicitly, one must expect that the resonance denominator may need to be multiplied by a phase factor $\exp(\mathrm{i}\phi)$. This was indeed observed in [22], where it was sufficient to take ϕ as constant. This point will be relevant in fitting 1^{--} and 2^{++} states to elastic data.

2.2 The continuation of amplitudes below thresholds

Consider as an example $\pi\pi \to KK$. It is necessary to continue this amplitude below threshold; in T-matrix language this is the analytic continuation of the T_{12} component. As a result, there are contributions to $\pi\pi$ elastic scattering from sub-threshold $\pi\pi \to KK \to \pi\pi$. However, caution is needed in making this continuation. The $\pi\pi \to KK$ amplitude is proportional to phase space $\rho_2 = \sqrt{1-4M_K^2/s}$ for the KK channel. Below threshold, this continues analytically as $\mathrm{i}\sqrt{4M_K^2/s-1}$. The analytically continued amplitude rises rather strongly below threshold. If one is not careful, this continued amplitude can make dominant contributions to elastic scattering below the inelastic threshold. This is counter-intuitive. A particular case arises for $f_2(1565)$, which couples strongly to $\omega\omega$. If one does nothing about the large sub-threshold $\omega\omega$ contribution, it produces big interferences wth the nearby $f_2(1270)$ and can distort rather severely the mass and width fitted to $f_2(1270)$.

The answer to this point is straightforward. Amplitudes above threshold contain form factors due to the finite radius of interaction forming the resonance. In [22], data on $\pi\pi \to KK$ were fitted empirically to an exponential form factor $\exp(-5.2k^2)$, where k is momentum in the KK rest frame in GeV/c; a study of $f_2(1565)$ in $\bar{p}p \to (\omega\omega)\pi^0$ at rest in Crystal Barrel data also requires a form factor above the $\omega\omega$ threshold of similar strength [34]. The analytic continuation can be evaluated below threshold using a dispersion integral. This is not an accurate procedure because of uncertainties in the $\pi\pi \to KK$ amplitude above the available mass range. However, the qualitative feature emerges that a rapidly falling form factor is required below threshold as well as above. In [22] this sub-threshold form factor was fitted to Kloe data with the result $\exp(-8.4|k|^2)$. This empirical cut-off will be adopted here for sub-threshold coupling to KK, $\eta\eta$ and $\omega\omega$.

2.3 Treatment of the 4π channel

The 4π phase space volume may be modelled [18] by the production of two resonances ($\rho\rho$ or $\sigma\sigma$):

$$\rho_{4\pi}(s) = \int_{4m_\pi^2}^{(\sqrt{s}-2m_\pi)^2} \frac{\mathrm{d}s_1}{\pi} \int_{4m_\pi^2}^{(\sqrt{s}-\sqrt{s_1})^2} \frac{\mathrm{d}s_2}{\pi} \frac{8|p||p_1||p_2|}{\sqrt{ss_1s_2}} \times |T_1(s_1)|^2 |T_2(s_2)|^2 FF(s)\,, \quad (6)$$

where p_1 and p_2 are momenta of pions from decays of each resonance in its rest frame, and p stands for the momenta of the ρ or σ in the centre of mass frame. In [23], extensive illustrations are shown of the dependence of $\rho_{4\pi}(s)$ on exponential form factors FF. These factors begin to play a significant role at ~ 1.45 GeV. A form factor

$$FF = \exp[-(s-1.45^2)] \quad (7)$$

is chosen in present work with s in GeV^2. If one were fitting data on $\pi\pi \to 4\pi$, this form factor would be rather important. However, for the present study of $f_0(1370)$ and $f_0(1500) \to \pi\pi$ it has only rather small effects within errors. This is because the $\Gamma_{4\pi}$ term in the Breit–Wigner denominator cuts off the $\pi\pi$ channel strongly at high mass; the $f_0(1370) \to \pi\pi$ amplitude is already quite small at 1.45 GeV, where the form factor begins. The $f_0(1500)$ is sufficiently narrow that the effect on the line-shape from 4π inelasticity is rather small. The one place where the form factor is important is in suppressing high mass contributions to $m(s)$.

Figure 1 shows $\rho\rho$ phase space as the dashed curve and $\sigma\sigma$ phase space as the chain curve. They are rather similar. Their relative contributions to each resonance are poorly known. The strategy here is to parametrise $\rho_{4\pi}$ empirically as

$$\rho_{4\pi} = \frac{\sqrt{1-16m_\pi^2/s}}{1+\exp[\Lambda(s-s_0)]}\,. \quad (8)$$

The parameters Λ and s_0 in the Fermi function of the denominator are optimised in the overall fit, with the result $\Lambda = 3.39\,\mathrm{GeV}^{-2}$, $s_0 = 3.238\,\mathrm{GeV}^2$. The result is shown by the full curve on Fig. 1.

The dispersive contribution $m(s)$ to Breit–Wigner amplitudes is evaluated numerically at 10 MeV steps of mass, and the programme interpolates quadratically in mass using the nearest 3 bins. The dispersion integral is the same for σ and all f_0's, except for (i) a subtraction at the resonance mass M, where the real part of the amplitude is zero, (ii) a scaling factor depending on the coupling constant to 4π. The sub-routine for doing the principal-value integral is available from the author if it is needed in other cases.

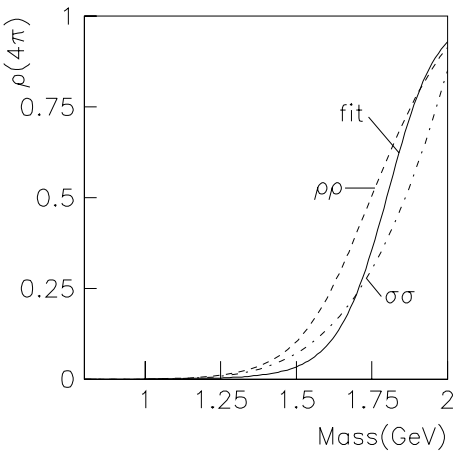

Fig. 1. 4π phase space for $\rho\rho$ (*dashed*), $\sigma\sigma$ (*chain curve*) and the fit adopted here (*full curve*)

2.4 Explicit equations for resonances

Formulae for the σ amplitude follow the same form as used in earlier work on the σ pole [32], except for the inclusion of $m(s)$ for 4π. Equations will be repeated here for completeness. The elastic amplitude is written

$$T_{11}(s) = N(s)/D(s)\,. \tag{9}$$

The numerator contains an Adler zero at $s = s_A \simeq 0.41 m_\pi^2$. For fits to BES data on $J/\Psi \to \omega\pi\pi$, the numerator is taken as a constant. Channels $\pi\pi$, KK, $\eta\eta$ and 4π will be labelled 1 to 4. The propagator of the σ is given by

$$D(s) = M^2 - s - g_1^2 \frac{s - s_A}{M^2 - s_A} z_s - m(s) - \mathrm{i} M \Gamma_{\rm tot}(s) \tag{10}$$

$$M\Gamma_1(s) = g_1^2 \frac{s - s_A}{M^2 - s_A} \rho_1(s) \tag{11}$$

$$g_1^2 = M(b_1 + b_2 s)\exp[-(s - M^2)/A] \tag{12}$$

$$j_1(s) = \frac{1}{\pi}\left[2 + \rho_1 ln_e\left(\frac{1-\rho_1}{1+\rho_1}\right)\right] \tag{13}$$

$$z_s = j_1(s) - j_1(M^2) \tag{14}$$

$$M\Gamma_2(s) = 0.6 g_1^2 F F_2^2(s) \tag{15}$$

$$M\Gamma_3(s) = 0.19 g_1^2 F F_3^2(s) \tag{16}$$

$$F F_i(s) = \exp\left(-\alpha |k|_i^2\right) \tag{17}$$

$$M\Gamma_4(s) = M g_4 \rho_{4\pi}(s)/\rho_{4\pi}(M^2)\,. \tag{18}$$

The value of α is 5.2 above thresholds and 8.4 below. The numerical coefficient 0.19 in (16) has been revised very slightly using the branching ratio fitted in Sect. 5 between $\eta\eta$ and $\pi\pi$. Values of b_1, b_2, A and M of (12) are given below in Table 6.

Resonance denominators for $f_0(1370)$, $f_0(1500)$ and $f_0(1790)$ are taken in the form of (1). An important detail is that the factor $(s - s_A)/(M^2 - s_A)$ of (10) is also used for Γ_1, Γ_2 and Γ_3 of $f_0(980)$, $f_0(1370)$, $f_0(1500)$ and $f_0(1790)$. That is, the Adler zero is included into the widths of all 0^+ resonances. Otherwise, parameters of $f_0(980)$ are taken initially from the BES determination [21], but are re-optimised within the sum of statistical and systematic errors when fitting present data. For $f_0(1500)$, the ratio Γ_2/Γ_1 is taken from the PDG average. For $f_0(1370)$, it is taken from [30], where extensive Crystal Barrel data on $\bar{p}p \to KK\pi$ are fitted. However, in practice the ratio Γ_2/Γ_1 has rather have little effect here; only the full width of the resonance is crucial. Values of Γ_3/Γ_1 are determined in Sect. 5, but again have little effect. The same ratios are used for $f_0(1790)$ as for $f_0(1500)$, in the absence of good data for $f_0(1790)$ in the KK channel; since the $f_0(1790)$ signal is weak, this is of no consequence. A trial has been made including into $f_0(1500)$ a weak coupling to $\omega\omega$ with a coupling constant a third of that for known decays to $\rho\rho$; the effect is negligible.

The $f_2(1270)$ is parametrised using

$$\Gamma_{2\pi}(s) = \Gamma_{2\pi}(M^2)\frac{k^2 D_2(k^2)}{k_r^2 D_2(k_r^2)} \tag{19}$$

$$\Gamma_{4\pi}(s) = \Gamma_{4\pi}(M^2)\frac{\rho_{4\pi}(s)}{\rho_{4\pi}(M^2)}\,. \tag{20}$$

Here k is the pion momentum in the f_2 rest frame and k_r is the value on resonance. The D_2 are Blatt–Weisskopf centrifugal barrier factors. Expressions for them are given in [18] at the end of Sect. 2.1; the barrier radius optimises at 0.75 ± 0.04 fm. The KK and $\eta\eta$ channels are treated in the same way. From the Particle Data book, $\Gamma_{2\pi}/\Gamma_{\rm tot} = 0.847$ on resonance. This value is not sufficiently accurate for fitting Cern–Munich data and is re-optimised to 0.802, since the relative heights of $\rho(770)$ and $f_2(1270)$ are important. This value may be accounting for a form factor in $\pi p \to \pi\pi p$ over the mass range between these two states.

The $\rho(770)$ is parametrised like $f_2(1270)$ using the D_1 centrifugal barrier factor. Its mass and width optimise at 778 and 153 MeV, close to PDG values. Trials were made including coupling to KK and $\omega\pi$, but had no significant effect on the fit to Cern–Munich data compared with uncertainties in the $\rho(1450)$ contribution.

The $f_2(1565)$ presents a problem. It is known from Crystal Barrel data [34] that it couples strongly to $\omega\omega$. It is expected to couple to $\rho\rho$ a factor ~ 3 more strongly. However, there are unfortunately no data to confirm this strong $\rho\rho$ coupling. Consequently it is dangerous to fit $f_2(1565)$ with the full s-dependence and $m(s)$ used for f_0's. In view of the fact the $f_0(1370)$ and $f_0(1500)$ line-shapes come out close to those of simple poles, it is therefore fitted with a Breit–Wigner amplitude of constant width, except that the $\omega\omega$ channel is added explicitly. This channel has an important effect in cutting off the line-shape above resonance, see Fig. 9 below.

Other 1^{--}, 2^{++}, 3^{--} and 4^{++} resonances are likewise fitted with Breit–Wigner amplitudes of constant width, for simplicity and ease of comparison with other work. In fitting elastic data, each amplitude is multiplied by a fitted factor $\exp(\mathrm{i}\phi)$. This is done rather than including mixing between all resonances, since the number of mixing terms becomes too large, and furthermore the resonances are poorly separated at present.

3 Fit to $\bar{p}p \to 3\pi^0$ at rest

Figure 2 shows the Dalitz plot for data in liquid hydrogen at rest; it is similar for gaseous hydrogen. [This figure is from [16] where $f_2(1520) \equiv f_2(1565)$]. Mass projections for both sets of data are shown in Fig. 3. There are conspicuous peaks due to $f_2(1270)$ and $f_0(1500) + f_2(1565)$. Narrow bands due to $f_0(980)$ are also visible. Ingredients in the fit are σ, $f_0(980)$, $f_2(1270)$, $f_2(1565)$, $f_0(1370)$, $f_0(1500)$ and a weak $f_0(1790)$.

P-state annihilation is best determined by data in gas, where it makes up 48% of events, close to the predicted 50% from calculations of Stark mixing [35]. This is mostly

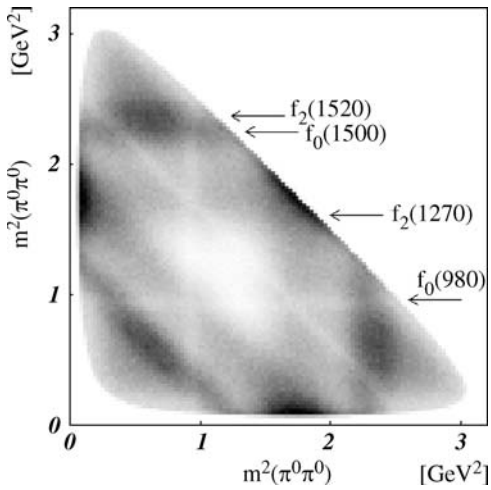

Fig. 2. The Dalitz plot for $\bar{p}p \to 3\pi^0$ in liquid hydrogen

annihilation with orbital angular momentum $L = 1$ in the transition, but a minor detail is that there is a little $L = 3$ production of $\pi^0 f_2(1270)$ and $\pi^0 f_2(1565)$. The fit to liquid data uses ${}^3P_1$ and ${}^3P_2$ components scaled down between gas and liquid by a factor which optimises at 0.155. The eventual P-state fraction is 12.8% in liquid.

A warning is that amplitudes for ${}^1S_0$, ${}^3P_1$ and ${}^3P_2 \to f_2(1270)$ or $f_2(1565)$ are poorly separated without using information from interferences between the three $\pi^0\pi^0$ contributions, which will be labelled 12, 23 and 13. The full angular dependence of amplitudes involves d-matrices which take account of rotations of axes between 12, 23 and 13 combinations:

$$ {}^3P_1, J_z = +1 : 3\cos\alpha \sin\theta\cos\theta - \sin\alpha(3\cos^2\theta - 1) \quad (21) $$

$$ {}^3P_1, J_z = 0 : \sqrt{2}[3\sin\alpha\sin\theta\cos\theta + \cos\alpha(3\cos^2\theta - 1)] \quad (22) $$

$$ {}^3P_2, J_z = 2 : \cos\alpha\sin^2\theta - \sin\alpha\sin\theta\cos\theta \quad (23) $$

$$ {}^3P_2, J_z = 1 : \sin\alpha\sin^2\theta + \cos\alpha\sin\theta\cos\theta\,. \quad (24) $$

For the 12 combination, θ is the angle in the $\pi^0\pi^0$ rest frame between π_1 and the recoil π_3; α_{1-3} are lab angles of 12, 23 and 13 combinations in their plane.

It turns out that ${}^3P_2$ annihilation dominates strongly over ${}^3P_1$ for both $f_2(1270)$ and $f_2(1565)$. Visible evidence for ${}^3P_2 \to f_2(1565)$ is the enhancement in Fig. 2 near the centre of each band just above 1500 MeV; this is how the Asterix collaboration discovered $f_2(1565)$ in gas data [36]. If ${}^3P_1$ annihilation to $f_2(1270)$ were large, there would be strong constructive interference between any two crossing bands near $\cos\theta = 0.6$; there is no sign of any such enhancement in the data.

3.1 The σ amplitude in $3\pi^0$ data

The σ is very broad, extending over the full $\pi\pi$ mass range from 0.27 to 1.74 GeV. Over such a large range, some s-dependence is to be expected in the numerator $N(s)$ of the production amplitude. The s-dependence required by the data is quite different between elastic scattering and the production process. An important feature of the data is an area of low intensity at the centre of the Dalitz plot of Fig. 2. Fitting this feature is delicate and demands s-dependence in $N(s)$.

Extensive trials have been made using a numerator for the σ amplitude of the form

$$ N(s) = A[1 + Bs + C/(s + s_0)]\,, \quad (25) $$

with $s_0 > 0$. What emerges is that (a) either complex B or complex C is definitely required and can fit the data well, (b) including both B and C over-parametrises the amplitude, i.e. strong correlations develop between B, C and s_0. It is better to tolerate a small increase in χ^2, so as to keep essential features clear with minimal correlations between fitting

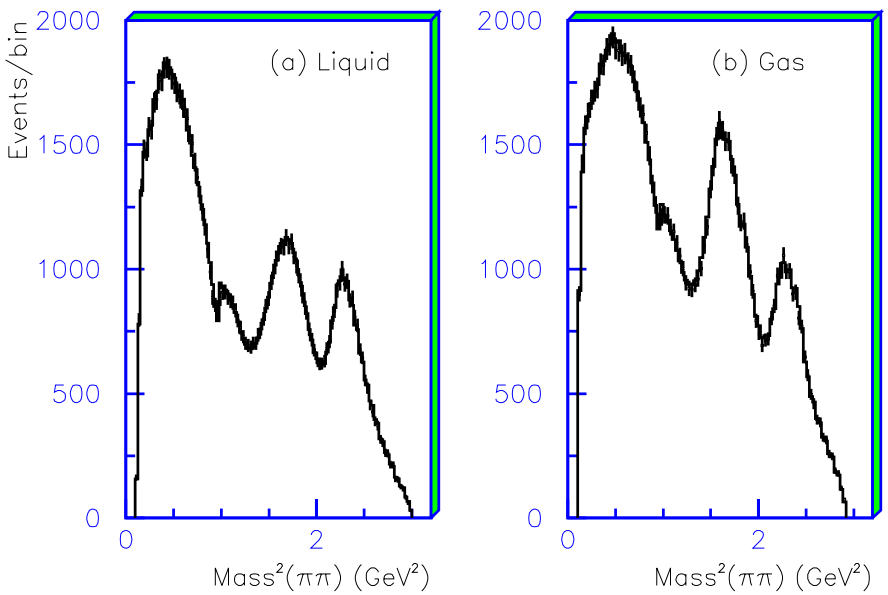

Fig. 3. Fits to the $\pi\pi$ mass proection in (**a**) liquid, (**b**) gas

parameters. Final fits were made with the form $A(1+Bs)$. Tests were also made including amplitudes arising from the opening of the KK threshold, i.e. $\propto T_{\pi K}$. These turned out to be negligible. A fit was also tried using a dependence on spectator momentum k given by the diffraction pattern of a black disk, but this gave a poor fit.

3.2 Prelimiminary remarks on the goodness of fit

The data are available to me only in the form of binned data, rather than individual events. Initial fits revealed that some edge bins have abnormally high χ^2. All lie immediately at the edge of the Dalitz plot. This is actually visible on Fig. 2. The same effect is observed for $\eta\eta\pi^0$ data. The obvious explanation of these bad bins is that the acceptance near the edge of the Dalitz plot may be incorrectly assessed. These bad bins have been removed without any significant effect on fitted amplitudes.

The resulting χ^2 is 2.83 per bin for $3\pi^0$ data in liquid, 2.85 in gas, 2.64 for $\eta\eta\pi^0$ in liquid and 2.70 in gas. A close inspection of discrepancies over the Dalitz plots reveals only an apparently random scatter, with no clear systematic effects. The mean χ^2 is 2.85 per bin. To allow for this, all values of χ^2 quoted in the paper are scaled down by a factor 2.85 so that the average χ^2 becomes 1 per bin. This is necessary for a correct assessment of the significance level of observations.

3.3 Fits including $f_0(1370)$

The Argand diagram for one $\pi^0\pi^0$ $^1S_0$ combination is shown in Fig. 4a; individual σ and $f_0(1370)$ components and their coherent sum are shown in other panels. At low mass, there is a conspicuous loop which is well fitted with the σ pole. This feature was correctly diagnosed by Ishida et al. [37]. They fitted only the $\pi\pi$ mass projection, so the present fit is much more accurate.

At higher mass, there is a loop due to $f_0(980)$. Here a detail needs explanation. Figure 5 shows the Argand diagram for $f_0(980)$ alone in $\pi\pi \to \pi\pi$. A mean kaon mass of 495.7 MeV is assumed. The KK inelasticity sets in very rapidly at threshold, and the peak inelasticity is at 1.010 GeV. Thereafter, the inelasticity parameter η rises again slowly, The result i s a definite 'dent' in the Argand diagam at 1.01 GeV.

Returning to Fig. 4a, there is a further loop at ~ 1300 MeV, followed by a large loop due to $f_0(1500)$. Figure 4a resembles closely fits made in 1996 [17]. The loop at 1300 MeV is the feature which is crucial to the existence of $f_0(1370)$. The vital questions are:

- (i) is this loop really needed?
- (ii) could it be fitted with σ and $f_0(1500)$ alone, without the need for $f_0(1370)$?

3.4 A suggestion of Ochs

Ochs has questioned whether the loop at 1300 MeV is an artificial feature of the way amplitudes are parametrised

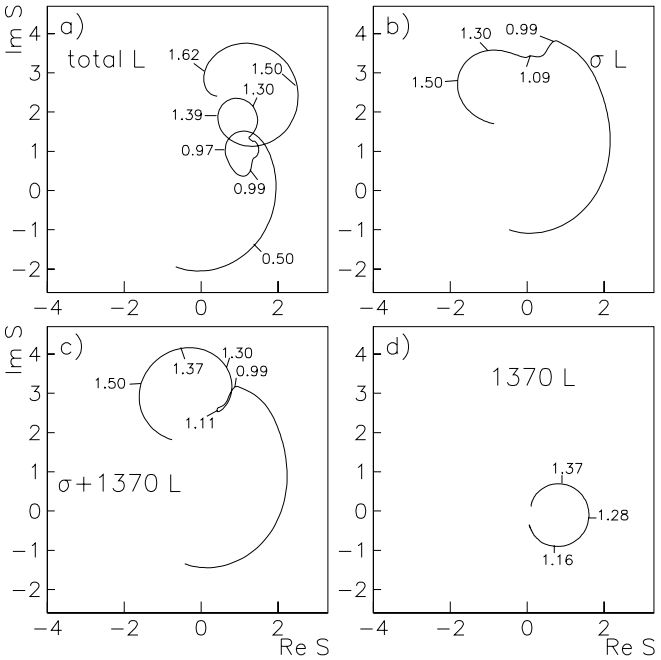

Fig. 4. Argand diagrams for the $\pi\pi$ S-wave in liquid hydrogen; masses are marked in GeV

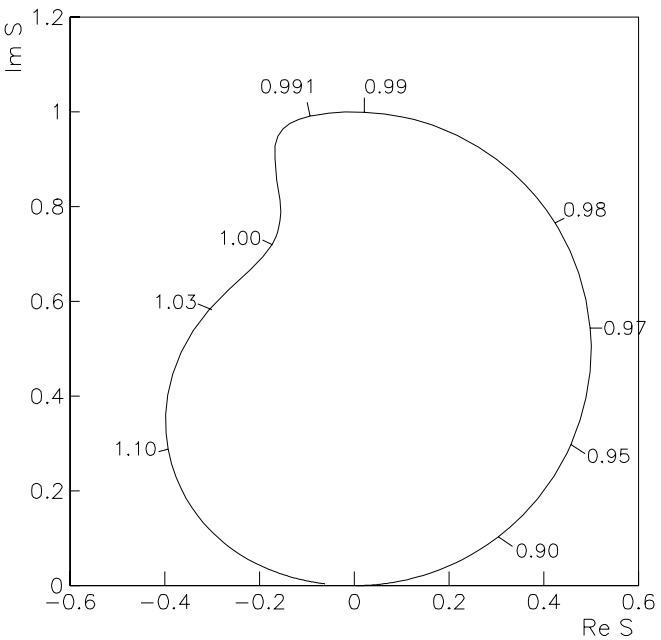

Fig. 5. The Argand plot for $f_0(980)$ alone; masses are marked in GeV

in terms of resonances (or backgrounds). My comment is that the parametrisation must be analytic; resonance forms used here satisfy this condition. Nonetheless, he has suggested fitting the $\pi\pi$ S-wave amplitude freely in magnitude and phase in bins of $\pi\pi$ mass, to see how definitively the data require the loop at 1300 MeV.

It is not possible to do this over the entire Dalitz plot, because of strong interferences between one low mass $\pi\pi$ contribution and two at higher mass. It is necessary to rely

on the strong σ loop at low mass and also the existence and parameters of the $f_0(1500)$, which is well known today from other data; it is also important to constrain the $f_0(980)$ within bounds set by BES II data.

It is, however, straightforward to fit the S-wave amplitude freely in magnitude and phase in bins from 1100 to 1460 MeV, i.e. over the 1300 MeV mass range. In this test, parameters of $f_0(1500)$ and $f_0(980)$ are allowed to reoptimise within the narrow ranges allowed by other data. For the σ, coefficients A and b of $N(s)$ are set free, but hardly move because they are determined by elastic data. Results are shown in Fig. 6 by crosses (indicating errors). Deviations from the fit of Fig. 4a, shown by the full curve, are barely above statistics, except for the third point (labelled 3) which moves by ~ 2.5 standard deviations. The agreement between the binned fit and Fig. 4a rules out the possibility that the 1300 MeV loop is an artefact of the parametrisation. As one example, it is not possible to replace the 1300 MeV loop by a narrow cusp arising from interference effects; such a cusp will be illustrated below for the $\pi\pi$ D-wave.

3.5 Properties of the fitted $f_0(1370)$

The fitted dispersive contribution $m(s)$ for $f_0(1370)$ is shown in Fig. 7. Near 1300 MeV, it varies roughly linearly with s, like the term $(M^2 - s)$ in the Breit–Wigner denominator. However, $m(s)$ is a factor ~ 1.6 larger than $(M^2 - s)$, This in an unusual feature, showing that care is needed in treating the 4π threshold correctly. It also leads to some effects which had not been forseen.

The term $m(s)$ is directly linked to $M\Gamma_{4\pi}(s)$ by the dispersion relation (2) of Sect. 1. This relation is reproducing effects of the loop diagram of Fig. 8. Results are analogous to vacuum polarisation, and lead to renormalisation effects in the Breit–Wigner denominator if the magnitude of $\Gamma_{4\pi}$ is scaled up or down.

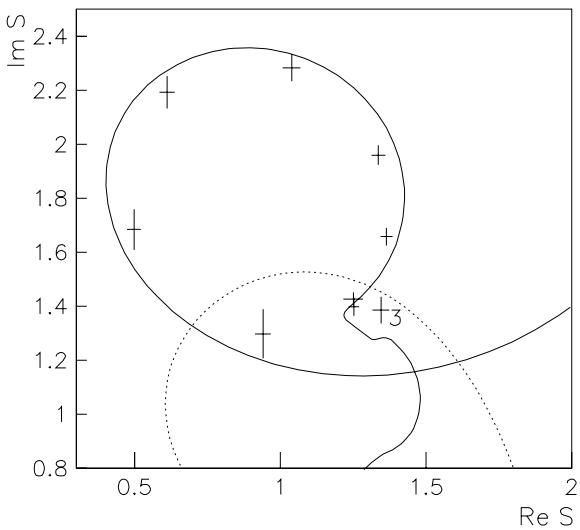

Fig. 6. The Argand diagram for the $\pi\pi$ S-wave (*full curve*) compared with free fits to magnitude and phase in nine 40 MeV wide bins of mass from 1100 to 1460 MeV (*crosses*)

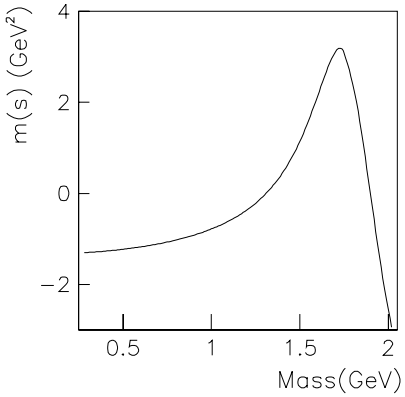

Fig. 7. The dispersive term $m(s)$ for $f_0(1370)$

A consequence in the combined fit to $\bar{p}p \to 3\pi^0$ and elastic data is that there is a tight constraint on the ratio $\Gamma_{2\pi}/\Gamma_{4\pi}$. Conversely, there is considerable flexibility in the absolute value of $\Gamma_{2\pi}$ which can be fitted. Table 1 shows pairs of values fitted to data; $\Gamma_{2\pi}$ and $\Gamma_{4\pi}$ are almost linearly related until $\Gamma_{2\pi}$ approaches zero, when the fit deteriorates rapidly. The final fit uses the lowest value of $\Gamma_{2\pi}$ giving a satisfactory fit, namely 325 MeV. A surprise is that $f_0(1370)$ is fairly elastic on resonance, though the inelasticity increases rapidly thereafter. Over the range of values shown in Table 1, there is almost no visible change in the line-shape of $f_0(1370)$. This is a renormalisation effect. It is illustrated in Fig. 9b for two widely different values of $\Gamma_{2\pi}$.

3.6 Lineshapes

Figure 9 shows the line-shapes of σ, $f_0(1370)$, $f_0(1500)$ and $f_2(1565)$ in $\pi\pi$ elastic scattering. The $f_0(1370)$ is almost

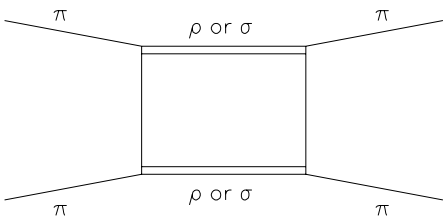

Fig. 8. The dispersive term $m(s)$ for $f_0(1370)$

Table 1. Parameter variations with $\Gamma_{2\pi}$ of $f_0(1370)$; units are GeV

$\Gamma_{2\pi}$	M	$\Gamma_{4\pi}$	$\Gamma_{4\pi}/\Gamma_{2\pi}$	χ^2
0.80	1.3113	0.1958	0.245	3519
0.65	1.3090	0.1472	0.226	3507
0.50	1.3093	0.1047	0.209	3505
0.40	1.3093	0.0766	0.192	3502
0.30	1.3096	0.0464	0.155	3500
0.25	1.3089	0.0318	0.127	3504
0.20	1.3114	0.0181	0.091	3512

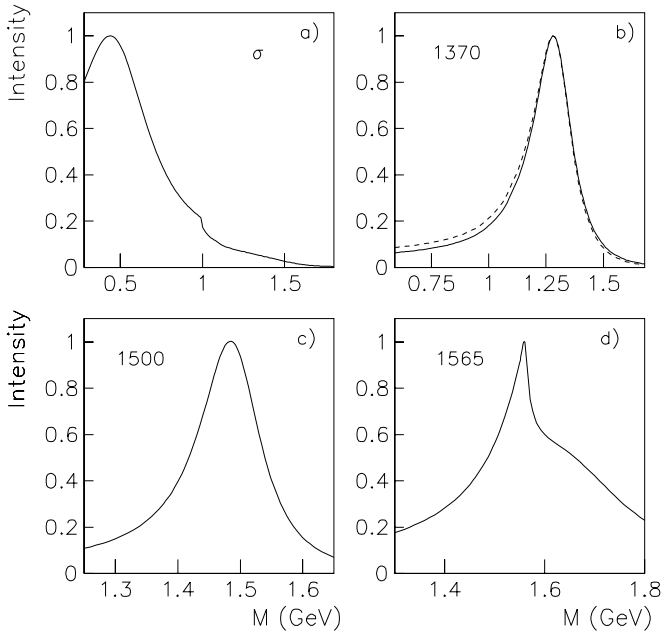

Fig. 9. Line-shapes of σ, $f_0(1370)$, $f_0(1500)$ and $f_2(1565)$ in $\pi\pi \to \pi\pi$, normalised to 1 at their peaks; the *dashed curve* for $f_0(1370)$ shows th e effect of changing $\Gamma_{2\pi}$ from 325 to 800 MeV

degenerate with $f_2(1270)$, which explains why it has been hard to observe experimentally. The peak of the intensity is at 1282 MeV in elastic scattering, though the phase shift goes through 90° at $M = 1309$ MeV. A similar pole mass is quoted by Anisovich and Sarantsev [30]: 1306 − i147 MeV for their solution 1 and marginally different for two alternative solutions. Although their parametrisation of amplitudes in terms of K-matrices is quite different to the approach adopted here, it is clear that their eventual fit

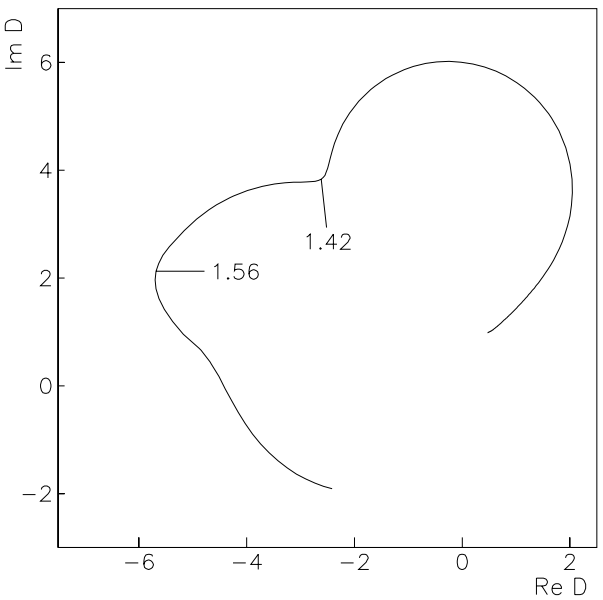

Fig. 10. The Argand plot for the $\pi\pi$ D-wave in $3\pi^0$ data in liquid hydrogen; masses are shown in GeV

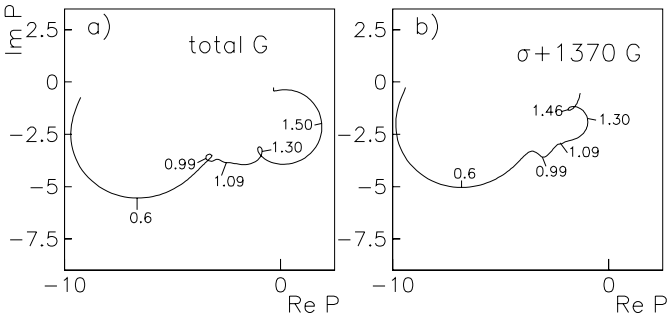

Fig. 11. Argand diagrams for the $\pi\pi$ S-wave in $^3P_1$; annihilation; masses are shown in GeV

is very similar to mine, and there is no serious disagreement between the two types of formalism.

The $f_0(1370)$ and $f_0(1500)$ are asymmetric, because the rapidly rising $\Gamma_{4\pi}$ in the Breit–Wigner denominator cuts off the intensity at high mass. The $f_2(1565)$ is likewise cut off strongly at high mass by the opening of the $\omega\omega$ threshold. It peaks exactly at the $\omega\omega$ threshold and has a half-width of 131 MeV below resonance.

3.7 The $\pi\pi$ D-wave

Figure 10 shows the Argand diagram for $^1S_0$ annihilation to the $\pi\pi$ D-wave. An interesting feature, already noted in [17], is the appearance of a cusp at 1420 MeV, almost midway between $f_2(1270)$ and $f_2(1565)$. No resonance can be accomodated at 1420 MeV by fitted magnitudes and phases of the amplitude. However, the PDG lists a state $f_2(1430)$. It seems likely that this is an artefact due to similar cusps in other reactions; it is an acute observation on the part of the experimental groups finding the effect.

3.8 P-state annihilation

Figure 11 shows Argand diagrams for $^3P_1$ annihilation to one $\pi\pi$ S-wave combination. The result comes almost purely from data in gas. There is some similarity to results in liquid, but definite differences; for example, the $f_0(980)$ contribution is almost negligible. There is again a loop near 1300 MeV in Fig. 11b. However, interference between $f_0(1370)$ and $f_0(1500)$ plays a decisive role in obtaining a good fit.

3.9 Fits without $f_0(1370)$

The entire fit has been re-optimised without $f_0(1370)$, refitting all parameters. The result is that (renormalised) χ^2 increases for $3\pi^0$ data in liquid by 1040, and by 1088 for data in gas. So the significance level of $f_0(1370)$ is slightly over 32 standard deviations in liquid and close to 33 in gas. These are essentially independent, since $^1S_0$ annihilation to $f_0(1370)$ is determined almost purely by liquid data and $^3P_1$ annihilation by gas data.

Attempts were made to improve the fit using different parametrisations for the σ, e.g. $N(s) \propto A[1 + C/(s + s_0)]$; however, that choice actually gave a slightly worse fit and other types of fit gave no significant improvement.

Figure 12 shows the resulting Argand diagrams for the $\pi\pi$ S-wave in (a) liquid, (b) gas. The fit tries to remedy the situation by using the σ amplitude as a replacement for $f_0(1370)$; the main latitude lies in increasing the inelasticity of σ to 4π. This fails because the amplitude cannot move round the required loop quickly enough, resulting in a very poor χ^2; one can see on Fig. 12 that the size of the loop at 1300 MeV has increased compared with that of Fig. 4. For the σ amplitude, the inelasticity to 4π rises slowly over the entire mass range 1200 to 2100 MeV. This produces a slow loop on the Argand diagram, see Fig. 4b for liquid (L). It is not possible to fit the narrow $f_0(1370)$, whose full-width at half-maximum is 207 MeV, with this slow loop.

Tornqvist [27, 28] has remarked that the dispersive contribution $m(s)$ to the σ amplitude could induce a second σ pole near the 4π threshold. All fits have been examined for such a pole, but there is no trace of it in any fit.

The conclusion is that a narrow $f_0(1370)$ is highly significant. However, one should not rely purely on χ^2. What adds considerable confidence is that fitted values of mass and width are in excellent agreement between two almost independent determinations in liquid data and gas. The value of $\Gamma_{2\pi}$ is held fixed at 325 MeV in both cases. Then the fitted value of $\Gamma_{4\pi}$ on resonance changes by only 4 MeV. Parameters are shown in Table 2. One must add a systematic error common to both determinations; the systematic errors shown in Table 2 cover the entire range of all observed fits to the six sets of data with any parametrisation of $N(s)$ for the σ amplitude.

For those who wish to reproduce $f_0(1370)$ and $f_0(1500)$ with less elaborate formulae than used here, the advice is to aim to reproduce the peak and half-heights of Table 2.

A further test has been made removing the phase variation of $f_0(1370)$. There is an increase in χ^2 of 165, i.e. nearly 13 standard deviations. However, the magnitude of the fitted $f_0(1370)$ increases by a large amount and the σ component decreases. So the non-resonant $f_0(1370)$ is then obviously simulating a large part of the σ amplitude. This confuses the interpretation of this test.

3.10 $f_0(1370)$ line-shape in 4π

Figure 13a shows as the full curve the line-shape of $f_0(1370)$ in $\pi\pi \to \pi\pi$; the dotted curve shows the line-shape of a simple Breit–Wigner amplitude of constant width with the same mass and width on resonance. The dashed curves show estimates of what is predicted in $\pi\pi \to 4\pi$. There is some uncertainty concerning form factors at high mass. Fortunately these form factors play little role in fitting present data, because the amplitude in the 2π channel is already quite small at 1.45 GeV, where the form factor begins to have an effect. The three curves illustrate results using form factors $\exp -\alpha(s - 1.45^2)$ (with s in GeV^2); the

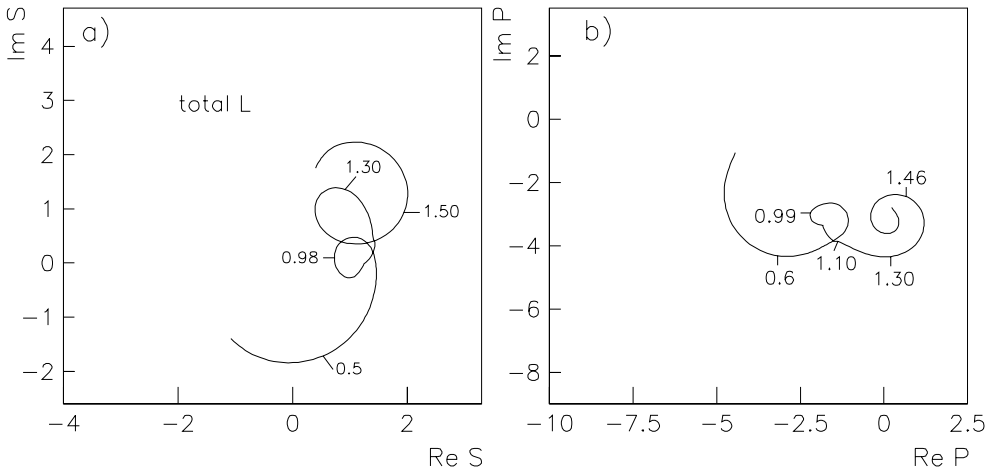

Fig. 12. Argand plots for the $\pi\pi$ S-wave in $3\pi^0$ data in liquid (L) and gas (G) with $f_0(1370)$ omitted; masses are shown in GeV

Table 2. Parameters in MeV for $f_0(1370)$ in (a) liquid, (b) gas, (c) combined, and $f_0(1500)$ for the combined fit

	(a)	(b)	(c)	(d)
$\Gamma_{2\pi}(M^2)$	325	325	325	127
M	1308	1312	$1309 \pm 1(\text{stat}) \pm 15(\text{syst})$	$1503 \pm 1(\text{stat}) \pm 6(\text{syst})$
$\Gamma_{4\pi}(M^2)$	53	56	$54 \pm 2(\text{stat}) \pm 5(\text{syst})$	$138 \pm 4(\text{stat}) \pm 5(\text{syst})$
Peak			1282	1485
Half-height			1165 and 1372	1418 and 1540
FWHM			207	122

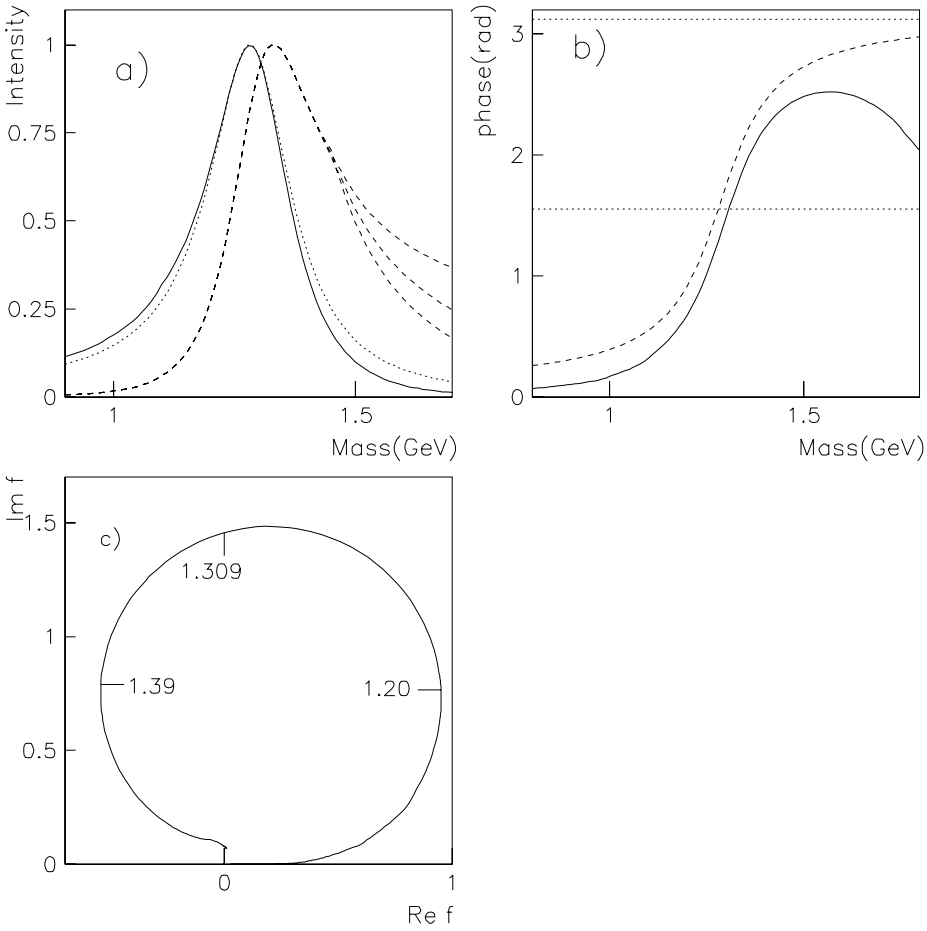

Fig. 13. (**a**) Line-shapes of $f_0(1370)$ for 2π (*full curve*), a Breit–Wigner amplitude with constant width (*dotted*), and for 4π (*dashed*), (**b**) the phase angle measured from the bottom of the Argand plot (*full curve*) and for a Breit–Wigner amplitude of constant width (*dashed*); *horizontal lines* mark phase shifts of $\pi/2$ and π, (**c**) Argand plot; masses are shown in GeV

top curve is for $\alpha = 0.5$, the central one for $\alpha = 1.0$ and the bottom one for $\alpha = 1.5$. These span a reasonable range of possibilities.

The main conclusion from these curves is that the peak of the resonance moves quite strongly between 2π and 4π channels because of the difference between $\rho_{2\pi}$ and $\rho_{4\pi}$. The 2π peak is at 1282 MeV and that in 4π is at 1331 MeV, i.e. a mass difference of ~ 50 MeV. However, if one works from the half-heights of the peaks, the difference is larger. For the 2π channel, half-height is at 1165 and 1372 MeV, i.e. a mean of 1269 MeV and a full-width at half maximum (FWHM) of 207 MeV. For the 4π channel, the corresponding half heights are 1241 and 1514 MeV, i.e. a mean of 1377 MeV and FWHM = 273 MeV. Further data on $\pi\pi \to 4\pi$ would be very valuable. In particular, data separating spins 0 and 2 would help greatly in clarifying the parametrisation of $f_2(1565)$. However, the analysis of these data must take into account contributions from $\sigma \to 4\pi$; that has not been done up to the present.

Figure 13c shows the Argand loop for $f_0(1370)$ in elastic scattering. The loop is cut off at the left by the effect of 4π inelasticity. It is remarkable that the loop is very close in shape to the circle given by a Breit–Wigner resonance of constant width. This provides some support for the constant width approximation which is frequently used. The resonance is behaving to first approximation as a simple pole with appropriate widths to 2π and 4π. However, Fig. 13b compares the phases for the s-dependent form of the amplitude (full curve) and constant width (dashed); these phases are measured from the origin of the Argand diagram. There is a sizable difference in phases, but only above the upper half-width of the resonance.

3.11 Parametrisation of $m(s)$

For convenience, an algebraic parametrisation of $m(s)$ is given here, to allow reconstruction of the amplitudes for $f_0(1370)$, $f_0(1500)$ and σ. It is not possible to find a simple accurate formula dealing with all three mass ranges. Instead, formulae will be given which are sufficiently accurate for extrapolations from the physical region to the poles. This implies weighting the fit to $m(s)$ in the vicinity of these poles.

The form of parametrisation is guided by the facts that (a) $\Gamma_{4\pi}$ is parametrised as a Fermi function, (b) the dispersive term is given approximately by the gradient of this function. Then $m(s)$ is expressed as a sum of terms

$$m(s) = \sum_i \left(\frac{a_i}{(s-s_i)^2 + w_i^2} - \frac{a_i}{\left(M_i^2 - s_i\right)^2 + w_i^2} \right) . \quad (26)$$

Table 3 gives numerical values of parameters. Note that the σ parametrisation applies only to the vicinity of the pole;

Table 3. Parameters fitting $m(s)$ in units of GeV

	$f_0(1370)$	$f_0(1500)$	σ
M	1.3150	1.5028	0.9128
a_1	3.5320	1.4005	17.051
s_1	2.9876	2.9658	3.0533
w_1	0.8804	0.8129	1.0448
a_2	−0.0427	−0.0135	−0.0536
s_2	−0.4619	−0.2141	−0.0975
w_2	−0.0036	0.0010	0.2801

Table 4. Pole position on various sheets

State	$\pi\pi$	4π	KK	$\eta\eta$	Pole (MeV)
$f_0(1370)$	+	+	+	+	$1299-\mathrm{i}187$
	+	−	+	+	$1309-\mathrm{i}43$
	+	+	−	+	$1293-\mathrm{i}180$
	+	+	+	−	$1292-\mathrm{i}177$
$f_0(1500)$	+	+	+	+	$1492-\mathrm{i}104$
	+	−	+	+	$1497-\mathrm{i}53$
	+	+	−	+	$1492-\mathrm{i}103$
	+	+	+	−	$1492-\mathrm{i}103$

if the full form of $m(s)$ is needed for the σ over the entire mass range, values may be read from Fig. 7 or the author will supply numerical tables.

A full account of pole positions on the many possible sheets is not helpful. The sheets may be labelled by the sign multiplying i. Table 4 then lists a representative set for $f_0(1370)$ and $f_0(1500)$. One sees immediately that the sign attached to i for KK and $\eta\eta$ has little effect on the pole position, because these inelasticities are small. What matters are the signs of i for $\pi\pi$ and 4π sheets. The imaginary part of the pole position changes substantially when the sign for the 4π sheet changes. This is a familiar effect of a strong inelastic channel. The experimental line width is close to the average of the results for the two 4π sheets.

4 Fits to elastic scattering

Four sources of information on elastic scattering are fitted simultaneously with production data. The first are Cern–Munich data from $\pi p \to (\pi\pi)n$. Secondly, K_{e4} data of Pislak et al. are included and constrain the $\pi\pi$ S-wave phase shifts up to 382 MeV [38]. Thirdly, Caprini et al have made a prediction of $\pi\pi$ phases using the Roy equations [39]. Their prediction up to 925 MeV is included with errors which are adjusted to give $\chi^2 = 1$ per point. These predictions are particularly important in constraining the scattering length and effective range. Amplitudes for $\pi\pi$ isospin 2 amplitudes are also included, and parametrisations are given below. Fourthly, BES II data on $J/\Psi \to \omega\pi^+\pi^-$ provide an accurate parametrisation of the σ pole, as discussed in [32]. The prediction of the lower side of the σ pole from the Roy equations is precise, but the BES data determine the upper side more accurately because of effects arising from the sub-threshold KK and $\eta\eta$ contributions.

In fitting Cern–Munich data, $J^P = 0^+$ contributions are included from σ and f_0's at 980, 1370, 1500, 1790, and 2020 MeV; the last of these is above the mass range of data, which finish at 1.89 MeV, but it needs to be included because of its large width. The $f_0(1710)$ is dominantly $s\bar{s}$ and is not expected to contribute strongly; any possible contribution is absorbed into the parameters of $f_0(1790)$.

Contributions are allowed for $J^P = 1^-$ from ρ's at 770, 1450, 1700, 1900 and 2000 MeV, although the $\rho(2000)$ is included only for completeness. For spin 2, $f_2(1270)$ plays a dominant role, but $f_2(1565)$ is definitely needed, as is some contribution from either or both of $f_2(1920)$ and $f_2(1950)$; the latter two however, cannot be separated cleanly. The $I = 2$ D-wave is also included, with formulae discussed in the next subsection.

For spin 3, $\rho(1690)$ plays a strong role, but there is definite evidence for some additional contribution from $\rho_3(1990)$. Finally, some definite but small contribution from $f_4(2040)$ is needed.

Before going into details, final fits to Cern–Munich moments are shown in Figs. 14 and 15. Panels are labelled by L, M of spherical harmonics fitted to data. The fit is quite adequate, but the eventual χ^2 is 3.13 per point. There is, for example, a definite systematic discrepancy with the $Y(51)$ moment, Fig. 15. This shows structure around 1270 MeV which cannot reasonably be attributed to interference with the low mass tail of $\rho(1690)$: the effect is too large. Near 1550 MeV, there are discrepancies with $Y2$ and $Y4$ moments, probably because of the effect of the $\rho\rho$ threshold on $f_2(1565)$; this is not explicitly included.

The fit to $f_0(980)$ is constrained within the linear sum of statistical and systematic errors quoted by BES for its mass, $g^2(\pi\pi)$ and $g^2(KK)/g^2(\pi\pi)$. The last of these is a useful constraint, but the fit does optimise the other two parameters within the BES errors, showing there is no conflict with Cern–Munich and Crystal Barrel data. The mass and width of the prominent $\rho(770)$ also need to be fitted freely, with the results $M = 778$ MeV, $\Gamma = 153$ MeV, in satisfactory agreement with PDG values. A small detail is that its coupling to 4π is included using on resonance the PDG estimate of the branching ratio; including this effect marginally improves the fit to the tail of the ρ above 1 GeV.

4.1 $I = 2$ amplitudes

There are experimental data on $\pi^+p \to (\pi^+\pi^+)n$ and hence the $I = 2$ S-wave amplitude. Wu et al. have calculated the expected inelasticity [40]. These two inputs have been fitted empirically as follows:

$$f(I=2) = (\eta \exp(2\mathrm{i}\delta) - 1)/2\mathrm{i}\,, \tag{27}$$

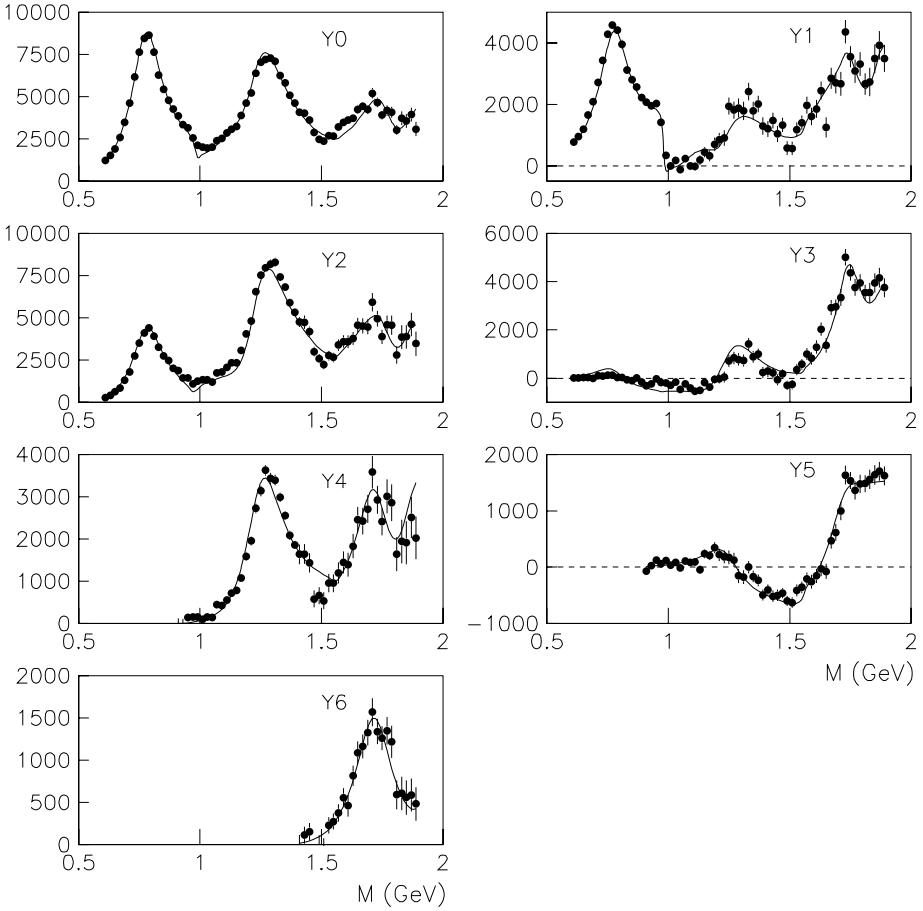

Fig. 14. Fit to Cern–Munich moments with $M = 0$

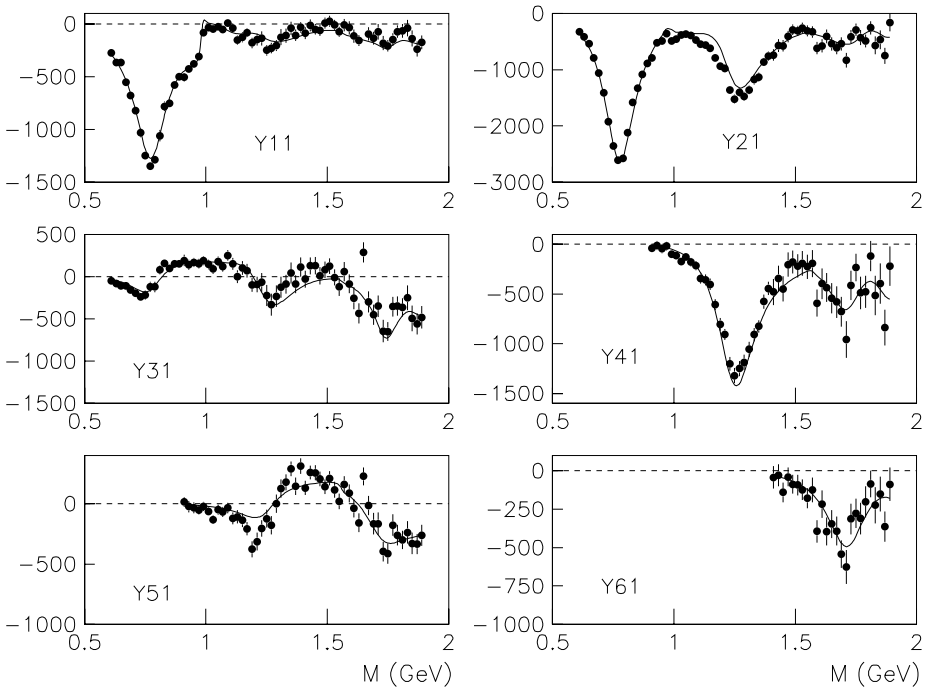

Fig. 15. Fit to Cern–Munich moments with $M = 1$

$$\eta = 1.0 - 0.5\rho_{4\pi}(s)\,, \tag{28}$$

$$\tan\delta = \frac{12.9\rho_{2\pi}}{11.9 + s/m_\pi^2}(a + bq^2 + cq^4 + fq^6)\,, \tag{29}$$

where q is pion momentum in the $\pi\pi$ rest frame, and $a = -0.0444$, $b = -0.12508$, $c = -0.00561$, $d = 0.00014$, all in units of pion masses.

The $I = 2$ D-wave has been studied carefully by Pelaez [41]. His formula for the phase shift δ is used. The elasticity η is set to 1 up to 1.05 GeV, and thereafter taken from the work of Wu et al. [40] as

$$\eta = 1 - 0.2(1.0 - 1.05^2/s)^3 . \quad (30)$$

The effect of this amplitude is very small in the present analysis.

4.2 Comments on fitted resonances

The $\pi\pi$ S-wave plays an important role in fitting moments with $L = 0$, 1, 2 and 3. The value of $\Gamma_{2\pi}$ for $f_0(1500)$ is well determined and significantly larger than has been generally assumed. Values of $\Gamma_{2\pi}$ are collected into Table 5. Values of χ^2 are renormalised downwards by a factor 3.13 in order to allow for the high χ^2 of the fit. The value of $\Gamma_{2\pi}$ for $f_0(1790)$ is not well determined because of overlap with the broad $f_0(2020)$. Argand diagrams are shown in Fig. 16.

Without $f_0(1370)$, a different type of solution can be obtained, but without the extra loop of Fig. 16 between 1.15 and 1.25 GeV. If the mass and width of $f_0(1500)$ are fitted freely, the χ^2 without $f_0(1370)$ is worse by 26. However, the width of $f_0(1500)$ goes up considerably, obviously because it is simulating missing $f_0(1370)$; also the mass goes down. If both mass and width of $f_0(1500)$ are held fixed, χ^2 is worse by 45 than with $f_0(1370)$ included.

Table 5. Parameters of fitted resonances; column 3 shows the (renormalised) change in χ^2 when the resonance is removed from the fit to Cern–Munich data

State	$\Gamma_{2\pi}$ (MeV)	$\Delta\chi^2$
$f_4(2040)$	16 ± 7	5.3
$\rho_3(1990)$	36 ± 8	12.4
$\rho_3(1690)$	44 ± 3	497
$f_2(1565)$	46 ± 14	33
$f_0(1500)$	61 ± 5	149

Either or both of $\rho(1450)$ and $\rho(1700)$ are required to reproduce $L = 1$ moments, but are poorly separated. One can remove either with a change in $\chi^2 < 10$. The mass and width of $\rho(1450)$ are taken from Babar data [42], where a conspicuous $a_1(1260)\pi$ signal is observed. The $\rho(1900)$ is fixed in width to the value 145 MeV, the mean of the two sets of Babar data [43]. It gives a significant improvement, but is not well separated from $\rho(2000)$. It may well be a radial excitation of $\rho(1450)$, but could also be a cusp effect due to the opening of the $\bar{p}p$ threshold. A fit using

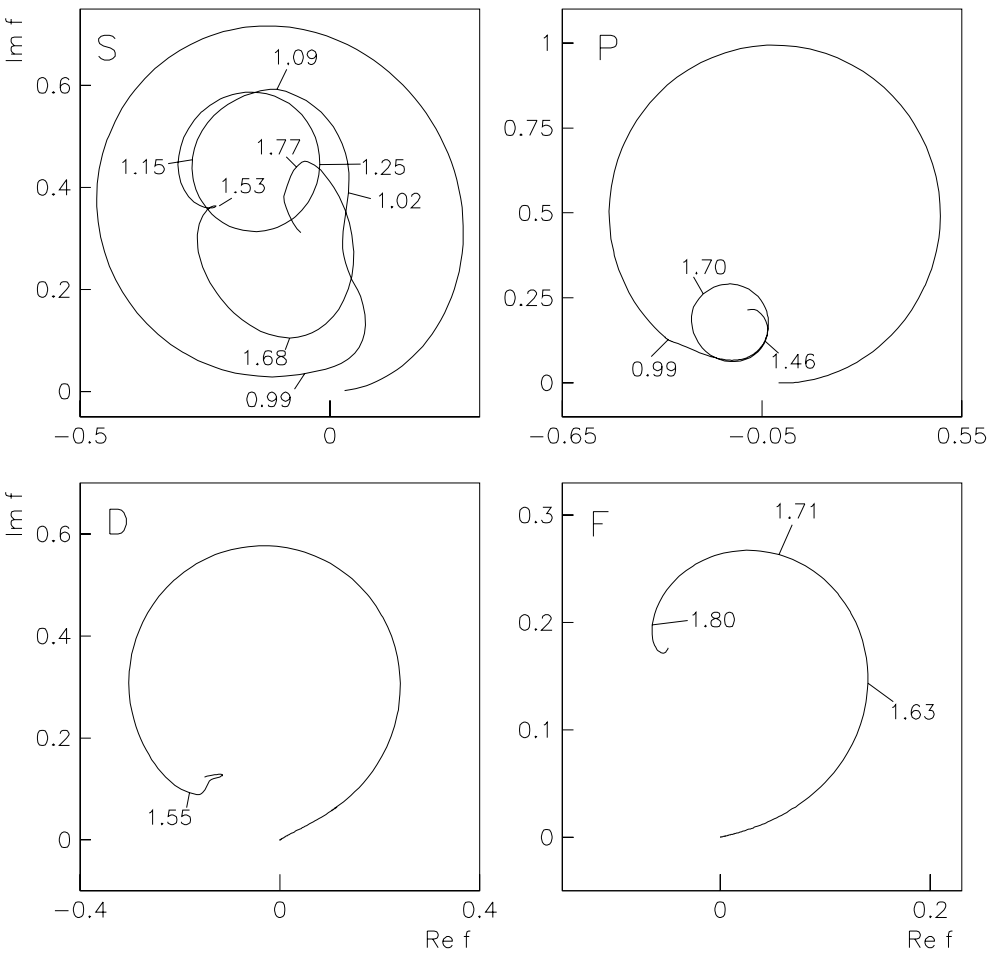

Fig. 16. Argand diagrams for $\pi\pi$ partial waves in elastic scattering

the narrow width of Frabetti et al. [44] is somewhat poorer. This raises the possibility of a resonance which has been attracted to the $\bar{p}p$ threshold; Frabetti et al may be sensitive to the threshold effect, while Babar data may be more sensitive to the resonance.

Spin 2 states contribute strongly to moments with $L =$ 2 to 5. The $f_2(1565)$ is definitely required but cannot be parametrised accurately because of missing information on $\Gamma_{4\pi}$.

The $\rho_3(1690)$ makes a strong contribution to moments with $L = 5$ and 6. Its optimum mass is 1709 ± 6 MeV. Reducing it to the PDG average of 1688.7 ± 2.1 does not affect the fit to $L = 6$ moments significantly, but does make the fit to $L = 5$ moments worse by 20 in χ^2. The value of $\Gamma_{2\pi}/\Gamma_{\rm tot}$ is 0.224 ± 0.032, in close agreement with the PDG value.

The fits shown in Figs. 14 and 15 include mixing between σ, $f_0(1370)$ and $f_0(1500)$. Figure 17 shows the fit to $Y0$, $Y2$, and $Y4$ with the mixing removed. Without this mixing, the fit to $Y2$ is not satisfactory, because interferences between $f_2(1270)$ and $f_0(1370)$ are not accurately fitted. Extra phase variations from the mixing play an important role. Such mixing is to be expected for strongly overlapping resonances.

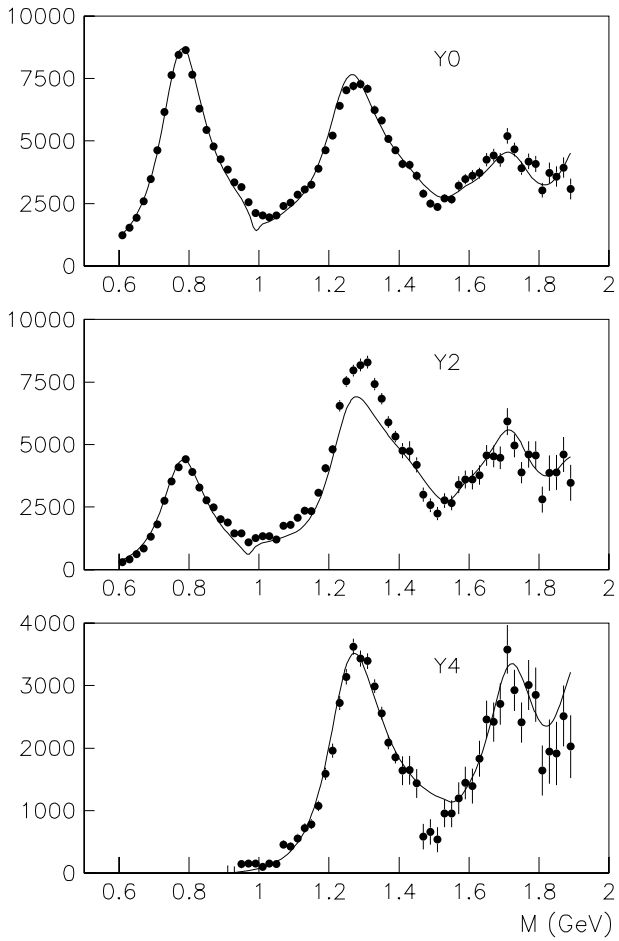

Fig. 17. The fit to Cern–Munich moments without mixing between σ, $f_0(1370)$ and $f_0(1500)$

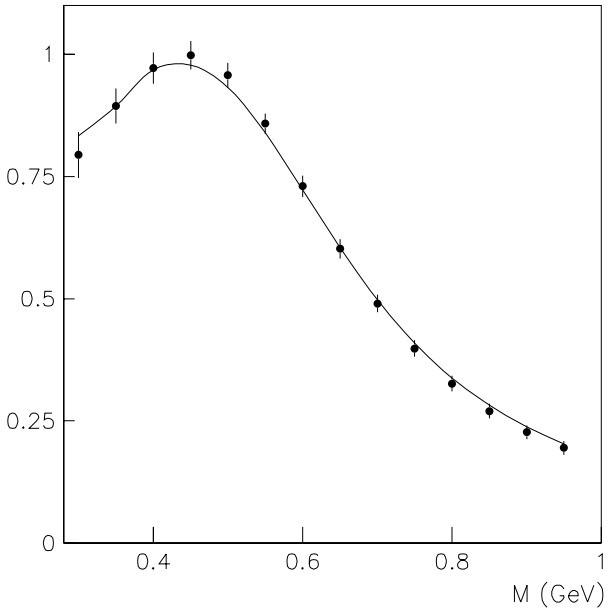

Fig. 18. The fit to the $\pi\pi$ mass projection of BES II data for $J/\Psi \to \omega\pi^+\pi^-$

Table 6. Parameters fitted to the σ amplitude in units of GeV

Parameter	Value
M	0.900
b_0	3.728
b_1	0.092
A	2.882
g_4	0.012

Figure 18 shows the fit to the $\pi\pi$ mass projection of BES data for $J/\Psi \to \omega\pi^+\pi^-$, normalised to 1 at the highest data point. The σ pole is at $470 \pm 30 - \mathrm{i}(260 \pm 30)$ MeV. These values have changed little from the work of [32]. Parameters fitted to the σ amplitude are shown in Table 6 in units of GeV. A parametrisation of $m(s)$ in the vicinity of the σ pole is shown above in Table 3.

5 Fits to $\bar{p}p \to \eta\eta\pi^0$ data

The $\eta\pi$ and $\eta\eta$ mass projections are shown in Fig. 19 for data in liquid hydrogen and gas. In (b) and (d) there are obvious peaks due to $a_0(980)$. In (a) and (c) there is a strong peak due to $f_0(1500)$ and a lower peak which is naturally attributed to $f_0(1370)$; it canno t be due to $f_2(1270)$, whose coupling to $\eta\eta$ is much too weak.

The ingredients in the fit are $a_0(980)$ and $a_2(1320)$, σ, $f_0(1370)$, $f_0(1500)$, $f_2(1270)$ and $f_2(1525)$. The $f_2(1270) \to \eta\eta$ contributes very little intensity, because of its small

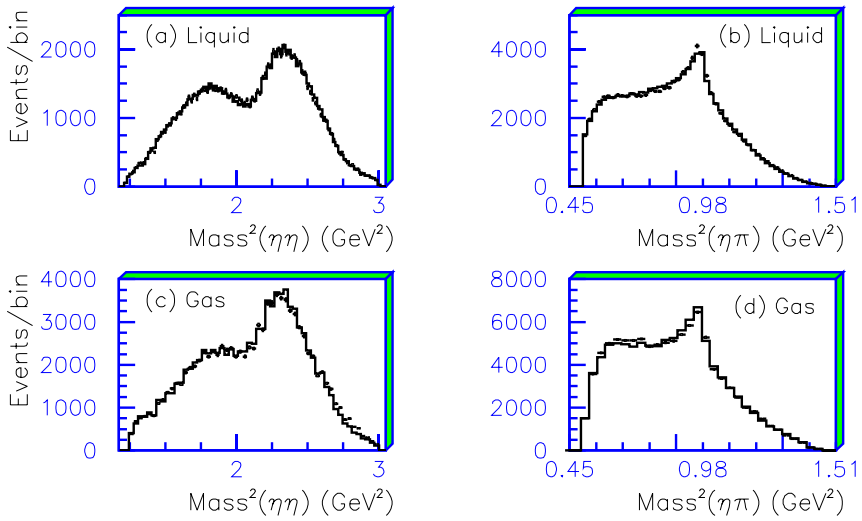

Fig. 19. Mass projections from data on $\bar{p}p \to \eta\eta\pi^0$ at rest in liquid hydrogen and gas; *points* show data and the *histogram* shows the fit

branching ratio, but it is desirable to include it in order to accomodate possible interference effects. This is done, fixing the branching ratios between $\eta\eta\pi^0$ and $3\pi^0$ data according to the PDG value for BR$[f_2(1270) \to \eta\eta]$/ BR$[f_2(1270) \to \pi\pi]$.

An earlier Crystal Barrel paper [16] has noted that there is evidence for $f_2(1525) \to \eta\eta$. However, its branching ratio is sufficiently low that it would not be seen in $3\pi^0$ data. This result is confirmed here, and the $f_2(1525)$ makes a large improvement to fitting $\eta\eta\pi$ data, $\Delta\chi^2 = 344$ summed over data in liquid and gas.

Additional fits have been made including the exotic $\pi_1(1400)$ in the $\pi\eta$ P-wave; however, it makes no significant contribution. The $a_0(1450)$ is above the available mass range in $\eta\pi$, but its low mass tail could contribute and this has been tried. However, the fits are no better than can be obtained by including form factors into the high mass tail of $a_0(980)$ in $\eta\pi$ and KK channels. Incidentally, the decay channel $a_0(980) \to \eta'\pi$ is included, assuming that the ratio $g^2[a_0(980) \to \eta'\pi]/g^2[a_0(980) \to \eta\pi] = (0.6/0.8)^2$, as predicted by the pseudoscalar mixing angle. This does improve the fit significantly, but needs further study for $\bar{p}p \to \eta\pi^0\pi^0$, where the $a_0(980)$ signal is more distinct.

The Argand diagram fitted to the $\eta\eta$ S-wave is shown in Fig. 20. There is a distinct cusp between $f_0(1370)$ and $f_0(1500)$. Masses and widths fitted to both resonances are entirely consistent with $3\pi^0$ data.

Without $f_0(1370)$ in the fit, the σ amplitude makes some contribution to replacing it. However, χ^2 is worse by 317 for liquid data, i.e. > 17 standard deviations, and 68 for data in gas, > 8 standard deviations. The significance level in liquid is high and confirms that the peak at ~ 1300 MeV in $\eta\eta$ cannot be fitted adequately with the σ contribution alone. This result by itself is sufficient to show the existence of $f_0(1370)$, but the determination of its mass and width are much poorer than from $3\pi^0$ data.

The fit determines the branching ratio of $\sigma \to \eta\eta$ compared with $\sigma \to \pi^0\pi^0$. There is, however, a substantial error which arises from interferences between the three

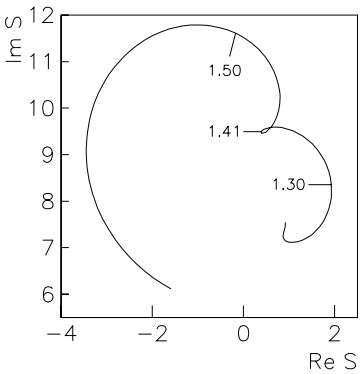

Fig. 20. The Argand diagram for the $\eta\eta$ S-wave in $\eta\eta\pi^0$ data in liquid; masses are shown in GeV

$\pi^0\pi^0$ contributions in $3\pi^0$ data. The σ contribution is the largest one to $3\pi^0$ data, and is subject to some flexibility depending on the precise s-dependence of the amplitude. There is a subtlety concerning the evaluation of the branching ratio. In the $3\pi^0$ data, the integrated intensity comes not only from the three individual $\pi\pi$ combinations 12, 23 and 13, but also from interferences between them. These interferences are quite large. What one needs is the branching ratio of an isolated resonance without these interferences. Putting this point in a different way, the resonances have specific coupling constants g^2 to each decay channel. One needs to derive these allowing for the fact that the three combinations interfere in the integrated intensity. This is done by evaluating intensities with and without these interferences. The result is

$$\frac{g^2(\eta\eta)}{g^2(\pi\pi)} = 0.19 \pm 0.05\,, \tag{31}$$

in close agreement with the earlier determination of [22], namely 0.20 ± 0.05.

Branching ratios for $f_0(1500)$ and $f_0(1370)$ to $\eta\eta$ compared with $\pi\pi$ are subject to the same large uncertainty

arising from the range of possible fits of σ to $3\pi^0$ data. Results are

$$\Gamma[f_0(1500)\to\eta\eta]/\Gamma(f_0(1500)\to\pi\pi]=0.135\pm0.04\,, \tag{32}$$

$$\Gamma[f_0(1370)\to\eta\eta]/\Gamma(f_0(1370)\to\pi\pi]=0.19\pm0.07\,. \tag{33}$$

6 Refitting data on $J/\Psi\to\phi\pi^+\pi^-$

These data provided earlier evidence for $f_0(1370)$ [21]. They are refitted here using for σ, $f_0(1370)$ and $f_0(1500)$ the formulae of Sect. 2 and the parameters determined here. The fit to $\phi\pi\pi$ data is displayed in Fig. 21, retaining the layout of the BES publication for comparison. Data on ϕKK are refitted simultaneously, but changes are

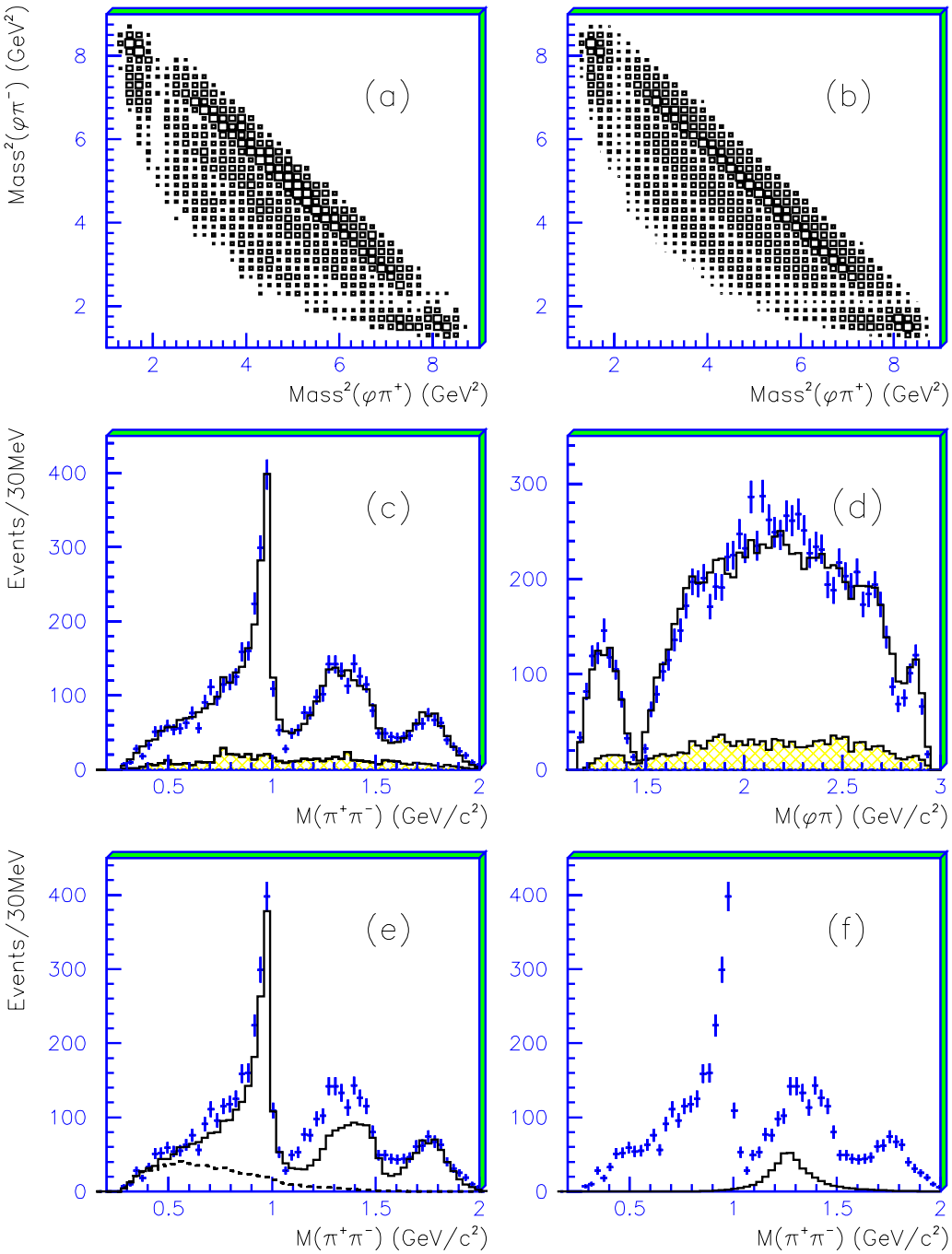

Fig. 21. Fit to BES II data on $J/\Psi\to\phi\pi^+\pi^-$. (**a**) Dalitz plot from data; (**b**) fitted Dalitz plot; (**c**) $\pi\pi$ mass projection and fit (*upper histogram*); experimental background is shown by the *lower histogram*; (**d**) fit to the $\phi\pi^+$ mass projection with the same format as (**c**); (**e**) the coherent sum of 0^+ contributions (*full histogram*); the *lower histogram* shows the σ component; (**f**) the contribution from $f_2(1270)$

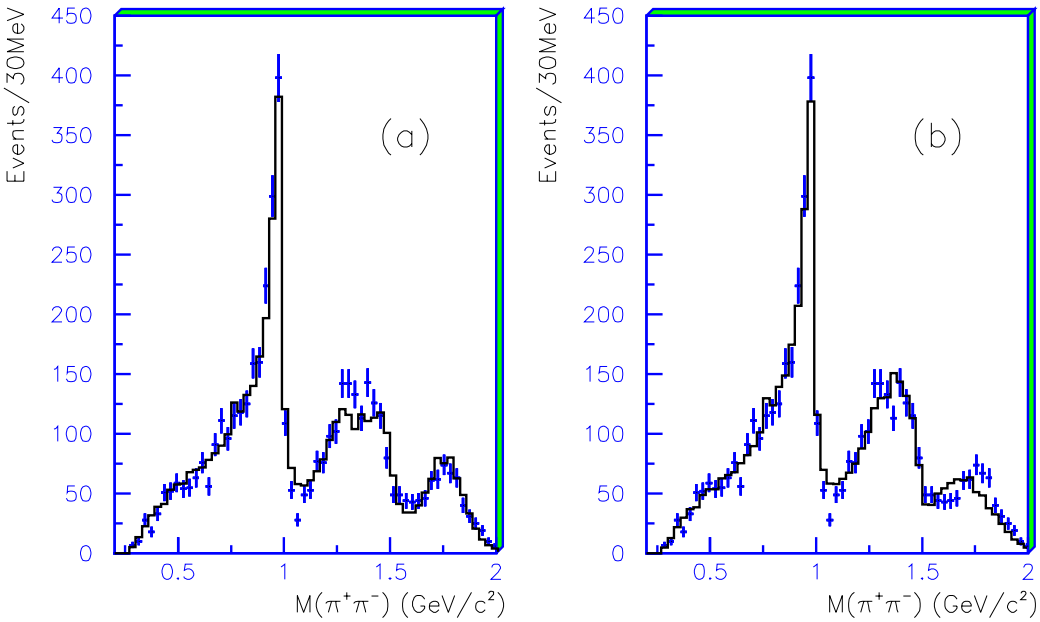

Fig. 22. (**a**) Fit to $\phi\pi\pi$ data without $f_0(1370)$; (**b**) the fit with a very broad 0^+ signal at 1650 MeV interfering destructively with $f_0(1500)$

barely visible on figures and will therefore not be shown here.

Technical details are as follows. It is important to constrain the branching ratios of $f_2(1270)$ and $f_0(1500)$ between KK and $\pi\pi$ within one standard deviation of PDG averages, so as to stabilise the fit to ϕKK data. The new σ parametrisation replaces the previous one, but has almost no effect: a 0.7 standard deviation change in log likelihood; there are much larger changes from reparametrisation of $f_0(1500)$ and $f_0(1500)$. The $\sigma \to KK$ contribution is very small and has little effect on the fit.

A reminder is necessary concerning the $\phi\pi\pi$ data. The BES analysis located a peak in $\phi\pi$ at 1500 MeV, arising from the triangle graph due to $J/\Psi \to K^+K^-\pi^+\pi^-$, followed by rescattering $KK \to \phi$. This was eliminated by a kinematic cut, creating the dips in the $\phi\pi$ mass spectrum of Fig. 21d at 1.5 and 2.8 GeV.

There is a peak at 1350 MeV in the $\pi\pi$ mass projection (c) attributed to interference between $f_2(1270)$, $f_0(1370)$ and $f_0(1500)$. The new fit is shown by the upper histogram; the lower one shows experimental background. The fit is marginally poorer than that of the BES publication, which had the freedom to optimise the mass of $f_0(1370)$ to 1350 ± 50 MeV and the width to 265 ± 40 MeV. It resulted in an $f_0(1370)$ contribution larger than $f_0(1500)$, though both were needed. Their roles are now reversed, with a 4.6% intensity contribution to $\phi\pi^+\pi^-$ from $f_0(1370)$ and a 6.1% contribution from $f_0(1500)$. On Fig. 21e, the full histogram shows the coherent sum of $J^P = 0^+$ contributions and the lower dashed histogram the σ contribution. Figure 21f shows the $f_2(1270)$ contribution. It is cleanly separated from 0^+ by angular distributions for production and decay of resonances.

Figure 22a shows the fit without $f_0(1370)$. The narrow $f_0(1500)$ is unable to compensate via interferences with σ, $f_2(1270)$ and $f_0(980)$ and the resulting fit is visibly poor. The fit is worse than Fig. 21 by 34.8 in log likelihood, i.e. > 8 standard deviations. This is sufficient to confirm the presence of $f_0(1370)$, but not enough to influence its fitted mass and width.

There is evidence that the $f_0(1370)$ is resonant. If its phase variation is artificially suppressed, leaving the lineshape unchanged (even though the resulting amplitude is non-analytic, therefore illogical), the fit is worse by 12.4 in log likelihood, ~ 5 standard deviations.

It has been suggested that the $f_0(1790)$ in BES data might be eliminated by fitting a broad $J^P = 0^+$ $\pi\pi$ signal with which $f_0(1500)$ interferes destructively, producing an interference minimum at ~ 1600 MeV. This suggestion was based on the possibility that the high mass tail of the σ might contribute strongly. That now appears illogical, since the σ amplitude falls rapidly with increasing s and is already small at 1 GeV.

The suggestion has been tested by fitting with a broad component with a width 1000 MeV and an optimised mass of 1650 MeV. Figure 22b shows the poor fit. It is of course possible to tune the width of this broad component to a lower value and produce a reasonable fit. However, it makes little sense to invent a new broad component when there is independent evidence for $f_0(1790)$ with consistent parameters in $J/\Psi \to \gamma(4\pi)$ data from both Mark III [45] and BES I [46]. Data on $J/\Psi \to \gamma\omega\phi$ [47] exhibit a striking 0^+ peak at 1812 MeV, which is consistent within errors with the upper side of $f_0(1790)$; the $\omega\phi$ threshold is at 1801 MeV.

7 Other data

Let us recall that the first evidence for $f_0(1370)$ came from data at the Argonne and BNL laboratories on $\pi\pi \to KK$ in the 1970 era. There is a distinct dip between the 1300 MeV peak and the narrow $f_0(980)$. Figure 10a of [22]

shows that without $f_0(1370)$ this dip cannot be fitted: the $f_0(980)$ is too narrow and interferences with the broad σ and $f_0(1500)$ fail to fit the data. Though these data alone at not sufficient proof of the existence of $f_0(1370)$, they are entirely consistent with parameters fitted here. The fit made in [22] has been rerun using the new parametrisations of the σ, $f_0(1370)$ and $f_0(1500)$ determined here. There is no significant change to conclusions of [22]. The analysis of Crystal Barrel data on $KK\pi$ channels by Anisovich and Sarantsev [30] finds $f_0(1370)$ mass, width and coupling constant in acceptable agreement with those reported here.

Data of Barberis et al. [48] on central production of $\pi\pi$ reveal quite different azimuthal distributions for $f_0(1370)$ and $f_0(1500)$, suggesting that two separate resonances are needed, whatever the nature of $f_0(1370)$.

8 The need for further analyses

Those who question the existence of $f_0(1370)$ should be concerned also about the existence of $a_0(1450)$. Despite its appearance in the summary table of the Particle Data Book, it is subject to the same questions about dispersive corrections as $f_0(1370)$. A fresh analysis is needed of data on $\bar{p}p \to \eta\pi^0\pi^0$, where it was discovered [49], including $m(s)$ into the parametrisation. It has also been observed in $\bar{p}p$ at rest $\to \omega\rho\pi^0$ in the $\omega\rho$ channel [50]. The threshold for this final state will contribute strongly to $m(s)$, as may the possible decay channel $a_0(980)\sigma$. A combined analysis of data on $\eta\eta\pi^0$ and $\omega\rho\pi^0$ is in progress and will be reported separately. If the $a_0(1450)$ survives, it is very likely to be a $q\bar{q}$ state, since none other is available for the isospin 1 component of the nonet in this mass range. If so, it is plausible that $f_0(1370)$ is likewise $q\bar{q}$ (mixed with the glueball).

Next, it is highly desirable to fit all existing data for the $J^{PC} = 1^{--}$ sector including dispersive corrections. A start has been made on this type of analysis by Weng et al. [51]. The greatest need is for data on $\pi\pi \to 4\pi$. These are needed to pin down details of the 4π final state with $J^{PC} = 0^{++}$, 1^{--} and 2^{++}. Such data were presented in a preliminary form by Ryabchikov at Hadron95, but have not been the subject of a full publication yet. The analysis including full dispersive effects is doubtless a major undertaking, but even limited information about the 4π channel would be very important.

Yet another example which may be affected strongly by dispersive effects is the $J^{PC} = 1^{-+}$ sector. There is substantial evidence for $\pi_1(1600)$ in decays to $b_1(1235)\pi$, $\eta'\pi$, $f_1(1285)\pi$ and $\rho\pi$. There is also evidence for structure in $\eta\pi$ at ~ 1400 MeV. This is close to the sharp thresholds for $b_1(1235)\pi$ and $f_1(1285)\pi$. It is still an open question whether there really is a resonant $\pi_1(1400)$, or whether it can be fitted adequately as a threshold effect. It is also possible that there is a resonance associated directly with these thresholds. What is needed is an analysis including dispersive effects due to the thresholds.

9 Concluding remarks

The $f_0(1370)$ is highly significant statistically in 5 sets of data: $\bar{p}p \to 3\pi^0$ at rest in liquid hydrogen and gas, corresponding data for the $\eta\eta\pi^0$ data channel, and $J/\Psi \to \phi\pi^+\pi^-$. Overall, it is statistically more than a 52 standard deviation effect. What is also important is that fitted parameters of $f_0(1370)$ agree remarkably closely between the $3\pi^0$ data in liquid and gas. There is weaker but consistent evidence for $f_0(1370)$ in $\pi\pi \to KK$.

The data cannot be explained by the high mass tail of the σ, because it is too broad. The requirement for a peak in data with a full width of 207 MeV requires an additional narrower state, identified here with the $f_0(1370)$. No such pole has appeared within the present parametrisation of $\sigma \to 4\pi$.

Dispersive contributions due to the opening of the 4π channel have large effects, renormalising the Breit–Wigner denominator. This severely limits the range of $\Gamma_{4\pi}/\Gamma_{2\pi}$ which can be successfully fitted to data. Despite the strong effect of the 4π threshold, the resonance loop on the Argand diagram is very close to a circle. This provides some justification for the common practice of fitting a Breit–Wigner resonance of constant width: the resonance behaves to first approximation like a simple pole. However, the phase is significantly affected once one reaches a mass more than one half-width above resonance. A simple Breit–Wigner amplitude is adequate for finding resonances; including $m(s)$ uncovers the dynamical effect of the threshold.

There are presently no significant inconsistencies in parameters of $f_0(1370)$ between sets of data on $\pi\pi$, KK and $\eta\eta$ channels. Wide variations of mass and width appear only in analyses of 4π data. However, those analyses do not presently include $\sigma \to 4\pi$, which is found here to play a large role. Unfortunately, these analyses need to be repeated including the σ contribution. Disagreements therefore exist only about schemes into which different authors wish to fit the known states. Those schemes should not be used as the basis for claiming that $f_0(1370)$ or any other resonance does not exist.

Some authors, for example Maiani et al. [29], raise concerns about mass differences between $f_0(1370)$, $K_0(1430)$ and $a_0(1450)$. It now appears that $f_0(1370)$ is nearly degenerate in mass with $a_1(1260)$, $f_1(1285)$ and $f_2(1270)$. So it appears to pose no particular problem. It is likely that the mass of $K_0(1430)$ is influenced by its strong coupling to $K\eta'$, whose threshold opens at ~ 1450 MeV. It is also known that $a_0(1450)$ appears only weakly in the $\eta\pi$ channel; it is likely that its mass is affected strongly by coupling to $\omega\rho$ and $a_0(1450)\sigma$ thresholds, just as the mass of $f_2(1565)$ is close to the $\omega\omega$ threshold, and much lower than the mass of $a_2(1700)$.

The present analysis of elastic data produces new quantitative estimates of $\Gamma_{2\pi}$ for $f_0(1500)$, $f_2(1565)$, $\rho_3(1690)$, $\rho_3(1990)$ and $f_4(2040)$. Data on $\pi\pi \to 4\pi$ would help greatly in confirming the present analysis, and parametrising more accurately 1^{--} states and $f_2(1565)$.

A final speculative remark emerges from the mixing between σ, $f_0(1370)$ and $f_0(1500)$, which appears to be

a necessity in fitting the elastic $\pi\pi$ data. This mixing suggests a possible analogy with chemical binding. In the hydrogen molecule, two configurations of protons and electrons mix. This is the familiar process of hybridisation. The lowest eigenstate may be calculated using a variational principle. The suggestion made here is that confinement involves a hybridisation due to overlapping of nearby resonant states. One linear combination of states with favourable SU(3) configuration moves down and other combinations are pushed up in energy, in a way analogous to formation of the covalent chemical bond. A similar variational principle is involved in the formation of a superconductor.

The relevance of such an idea to the confinement process itself is a matter of conjecture without calculations to support it. The idea is that there is feedback between the formation of resonances and a dynamic confinement, i.e. condensation. Such a mechanism would explain naturally why most of the huge number of possible molecular states are not observed: most of them are driven upwards and become a continuum.

Acknowledgements. It is a pleasure to thank Dr. Andrei Sarantsev for providing the Crystal Barrel data used here and for discussions about meson resonances in general over a period of many years. I am also grateful to Profs. V. Anisovich, G. Rupp and E. van Beveren for similar discussions. I wish to thank Prof. E. Klempt for providing Fig. 2 of unbinned Crystal Barrel data.

References

1. C.J. Morningstar, M.J. Peardon, Phys. Rev. D **69**, 034 509 (1999)
2. E. Klempt, hep-ph/0404270
3. E. Klempt, A. Zaitsev, Glueballs, hybrids, multiquarks, submitted to Phys. Rep. (2007)
4. W. Ochs, AIP Conf. Proc. **619**, 167 (2002)
5. W. Ochs, QCD06, Montpellier, France, July 3–7 (2006)
6. D. Cohen et al., Phys. Lett. D **22**, 2595 (1980)
7. A.J. Pawlicki et al., Phys. Rev. D **15**, 3196 (1977)
8. A. Etkin et al., Phys. Rev. D **25**, 1786 (1982)
9. C. Amsler et al., Phys. Lett. B **291**, 347 (1992)
10. M. Gaspero, Nucl. Phys. A **562**, 407 (1993)
11. A. Adamo et al., Nucl. Phys. A **558**, 13c (1993)
12. C. Amsler et al., Phys. Lett. B **322**, 431 (1994)
13. V.V. Anisovich et al., Phys. Lett. B **323**, 233 (1994)
14. V.V. Anisovich, D.V. Bugg, A.V. Sarantsev, B.S. Zou, Phys. Rev. D **50**, 1972 (1994)
15. D.V. Bugg, V.V. Anisovich, A.V. Sarantsev, B.S. Zou, Phys. Rev. D **50**, 4412 (1994)
16. C. Amsler et al., Phys. Lett. B **355**, 425 (1995)
17. A. Abele et al., Nucl. Phys. A **609**, 562 (1996)
18. D.V. Bugg, A.V. Sarantsev, B.S. Zou, Nucl. Phys. B **471**, 59 (1996)
19. B.D. Hyams et al., Nucl. Phys. B **64**, 134 (1973)
20. Particle Data Group, J. Phys. G **33**, 1 (2006)
21. M. Ablikim et al., Phys. Lett. B **607**, 243 (2005)
22. D.V. Bugg, Eur. Phys. J. C **47**, 45 (2006)
23. A.V. Anisovich et al., Nucl. Phys. A **690**, 567 (2001)
24. E.M. Aitala et al., Phys. Rev. Lett. **86**, 770 (2001)
25. M. Ablikim et al., Phys. Lett. B **598**, 149 (2004)
26. D.V. Bugg, Eur. Phys. J. C **37**, 433 (2004)
27. N.A. Tornqvist, Phys. Rev. Lett. **49**, 624 (1982)
28. N.A. Tornqvist, Z. Phys. C **68**, 647 (1995)
29. L. Maiani et al., Eur. Phys. J. C **50**, 609 (2007)
30. V.V. Anisovich, A.V. Sarantsev, Eur. Phys. J. A **16**, 229 (2003) and further references given there
31. M. Ablikim et al., Phys. Lett. B **603**, 138 (2004)
32. D.V. Bugg, J. Phys. G **34**, 151 (2007)
33. A.V. Anisovich, V.V. Anisovich, A.V. Sarantsev, Z. Phys. A **359**, 173 (1997)
34. C.A. Baker et al., Phys. Lett. B **467**, 147 (1999)
35. G. Reifenrother, E. Klempt, Nucl. Phys. A **503**, 886 (1989)
36. B. May et al., Phys. Lett. B **225**, 450 (1989)
37. M. Ishida et al., Prog. Theor. Phys. **104**, 203 (2000)
38. S. Pislak et al., Phys. Rev. D **67**, 072 004 (2003)
39. I. Caprini, I. Colangelo, H. Leutwyler, Phys. Rev. Lett. **96**, 032 001 (2006)
40. F.Q. Wu et al., Nucl. Phys. A **735**, 111 (2004)
41. J.R. Pelaez, hep-ph/0510215
42. B. Aubert et al., Phys. Rev. D **71**, 052 001 (2005)
43. B. Aubert et al., Phys. Rev. D **73**, 052 003 (2006)
44. P.L. Frabetti et al., Phys. Lett. B **578**, 290 (2004)
45. D.V. Bugg et al., Phys. Lett. B **353**, 378 (1995)
46. J.Z. Bai et al., Phys. Lett. B **472**, 207 (1999)
47. M. Ablikim et al., Phys. Rev. Lett. **96**, 162 002 (2006)
48. D. Barberis et al., Phys. Lett. B **474**, 423 (2000)
49. C. Amsler et al., Phys. Lett. B **333**, 277 (1994)
50. C.A. Baker et al., Phys. Lett. B **563**, 140 (2003)
51. Y. Weng et al., hep-ex/0512052